

RESEARCH ARTICLE

Effect of rotation and domain aspect-ratio on layer formation in strongly stratified Boussinesq flows

Susan Kurien^{ab*}, Leslie M. Smith^c

^a*Theoretical Division, Los Alamos National Laboratory, Los Alamos, NM 87545, USA;*

^b*New Mexico Consortium, Los Alamos, NM 87544, USA;*

^c*Departments of Mathematics and Engineering Physics, University of Wisconsin, Madison, WI, USA*

(Received 00 Month 200x; final version received 00 Month 200x)

We present a numerical study of layer formation in forced, rotating, stably stratified Boussinesq flows. All flows are strongly stratified such that the buoyancy timescale $1/N$ is much faster than the turbulence timescale. The Coriolis timescale $1/f$ is chosen to be comparable to the turbulence timescale or faster. Furthermore, all simulations are in an asymptotic parameter regime defined by quadratic potential enstrophy. The aspect-ratio of the domain is $\delta = H_d/L_d$ where H_d (L_d) is the vertical height (horizontal length) of the domain, and the Froude (Rossby) number are defined using vertical (horizontal) scale and a velocity scale, both based on the large-scale force. Two sets of simulations are studied, both with fixed Froude number $Fr = Fr_o \approx 0.002$. The first set of runs fixes $\delta = 1$ and varies the Rossby number $Fr_o \leq Ro \leq 32Fr_o$. These unit aspect-ratio runs show a transition from flow with a quasi-geostrophic component to a layered flow as the Rossby number is increased from $Ro = Fr_o$. The layering appears first in the wave component of the flow, but is gradually dominated by the vortical component for large-enough Rossby number. Partly motivated by mid-latitude geophysical flows, the second set of runs fixes the Burger number $Bu = Ro/Fr_o = N\delta/f = 1$ and varies the domain aspect-ratio $1/16 \leq \delta \leq 1$ (correspondingly $16 \geq N/f \geq 1$). Wave-mode layering is also present in the runs with $Bu = 1$ and $\delta < 1$, with vortical mode layering appearing only as $\delta < 1/4$. Comparing the two sets of simulations for fixed $N/f > 1$, energy is suppressed in the vortical mode component for the $\delta = f/N$ as compared to $\delta = 1$. In general, as N/f increases from unity, there is a steady increase in the relative energy in the vortical modes at sub-forcing scales, but the rate of increase is slower if the aspect-ratio is decreased simultaneously so as to keep $Bu = 1$. The characteristic scales of the wave and vortical modes are measured using correlation lengths in the vertical and horizontal. As N/f increases, the vortical mode thickness decreases as f/N while the wave mode thickness increases as $\simeq (N/f)^{1/2}$. The latter contribution may well provide a correction to the f/N behavior observed for scale measurements in prior studies. The study is a first attempt to systematically characterize how both external aspect-ratio δ and N/f determine the internal scales and aspect-ratios of the structures formed in such flows.

Keywords: Boussinesq; Rotating turbulence; Stratified turbulence; small aspect-ratio flows

1. Introduction

We consider strongly stratified flows, aiming to study the effects of varying rotation rate and domain aspect-ratio on the internal scales and aspect-ratios of the emerging layered structures. The stratification is quantified by a large-scale Froude number Fr , which is the ratio of a non-linear inverse timescale to the stratification frequency N . Similarly, the Rossby number measures the strength of the

*Corresponding author. Email: skurien@lanl.gov

Coriolis parameter f , which is twice the frame rotation rate, relative to the turbulence timescale. Our goal is to remain in a well-defined region of parameter space where intermediate sub-forcing scales are strongly influenced by buoyancy while the Rossby number Ro and domain aspect-ratio δ are varied. Therefore in these studies, $Fr \ll 1$ is (nearly) fixed across all flows. In addition to the non-dimensional parameters Fr , Ro and δ , the Burger number $Bu = Ro/Fr$ (alternatively defined as $(Ro/Fr)^2$ [1]) is thought to be an important indicator of flow structure. Broadly speaking, the internal (horizontal) deformation radius L at which $Bu = 1$, specifies the scale at which rotation effects balance those of stratification for a given vertical scale H [2]. $Bu > 1$ is thus characteristic of stratification-dominated flows. All the parameter definitions described thus far are scale-dependent and vary for a given flow depending on the scales chosen. For consistency and in order to maintain a tractable parameter space, all the above non-dimensional parameters in our study are based on the imposed large (forcing) scales, associated velocity, and the domain aspect-ratio. We justify this choice *a posteriori* by relating the global parameters to the internal (emergent) parameters.

Structure formation in strongly stratified and rotating flows has received much attention during the last several decades, for example, see [3–20]. These studies span the gamut from purely stratified flow to purely rotating flow, with and without significant small-scale turbulence, and with both unit and small domain aspect-ratio. It is known that stratification and nonlinear forcing (turbulence from various sources such as body-force, boundaries, baroclinic instability etc.) can play competing roles in that the former tends to force the flow into stable layers, while the presence of the latter might disrupt (overturn) such layers. Similarly, rotation forms a competing mechanism to stratification, tending to force the flow into columnar structures. Our particular focus is on the variability of layered structure in strongly stratified flows, due to changes in rotation and aspect-ratio. In order to isolate as much as possible these effects of interest, we chose to study flow in which the turbulence timescales are much slower than either the stratification or rotation frequencies so that the only competition to the stratification in the structure formation is rotation in variable domain aspect-ratios. Such a study might have relevance even to flow with weak to moderate turbulence. Recently, [21, 22] investigated layer formation in experimental studies of rotating and stratified, decaying grid turbulence. In [22], the integral length-scale in the vertical direction (one measure of the layer thickness) was observed to increase monotonically with f/N even while the turbulence decayed. This work suggests that some quantitative features of the layering may be independent of the strength of turbulence (relative to stratification or rotation) in the flow. In this spirit, we explore strongly stratified flows for variability in structure formation with respect to rotation and domain aspect-ratio, while suppressing the effects of turbulence.

In our work with $Fr \ll 1$, we explore a region of parameter space in which the potential vorticity is dominated by a linear term, with intent to ultimately make connection with theoretical results. The conservation of linear potential vorticity has been a cornerstone of theory and modeling beginning with the work of Ertel [23]. Charney [24] deduced the direction of energy and potential enstrophy fluxes and the energy scaling laws for quasi-geostrophic (QG) flows. The quasi-geostrophic model equations are precisely the mathematical statement of conservation of a linear potential vorticity, and can be rigorously derived using fast-wave averaging in the limit $Ro \sim Fr \rightarrow 0$ [25]. Linear potential vorticity is also associated with the limit $Fr \rightarrow 0, Ro = \mathcal{O}(1)$ which permits the so-called vertically sheared horizontal flows (VSHF) [9, 19, 25–27]. For $Bu = 1$, small aspect-ratio flows, [28] showed analytically that three-wave near-resonant interactions become sparse, thus inhibiting

the formation of VSHF that were observed to develop in the unit aspect-ratio simulations of [9, 19, 26, 27, 29]. In [30, 31], the utility of quadratic potential enstrophy (one-half the square of linear potential vorticity) was explored for deriving exact statistical flux laws and for constraining energy. In related work [32] studied the joint downscale fluxes of both potential enstrophy and energy in strongly rotating and stratified flows, highlighting the difference between such flows and two-dimensional turbulence. And in [33] we concluded that the flows with unity Burger number for even asymptotically small Ro and Fr are perhaps non-universal and depend on aspect-ratio. In the present work we use numerical simulations to complement these prior theoretical and computational results and to systematically explore the effects of domain aspect-ratio and rotation on structure formation and layering in strongly stratified flows. A novel feature of our study is the dissection of the layering phenomena by separating the trends in the wave and vortical components of kinetic energy, and attempting to correlate these to the structure formation. The linear potential vorticity limit might also be of use in studies of strongly rotating flows and the data analysis we present here may be helpful in those regimes as well.

Stratified flows in general have relevance to geophysical phenomena, though here we do not attempt to make direct connection with any particular geophysical application. To avoid confusion, we point out that our simulations should not be used to interpret the empirically measured Nastrom-Gage spectrum [34] of the mid-latitude atmospheric mesoscales. Spectral scalings studies to recover the Nastrom-Gage spectrum have included both numerical and phenomenological work [17, 20, 35], with consensus that the potential enstrophy in those regimes, while not directly measured, is quite likely not quadratic.

Section 2 follows with a discussion of the equations of motion and conservation laws. In section 3, we give the details of the simulations followed by discussion of the three levels of comparison of the data: 1) varying Ro for fixed Fr in unit aspect-ratio 2) varying aspect-ratio for fixed Fr and $Bu = 1$ and 3) decreasing aspect-ratio from unity to f/N for various fixed N/f . Section 4 presents calculations of integral length scales of both wave and vortical components and the internal aspect-ratios. We conclude with a summary of the work and some conjectures about how the global parameters Fr , Ro , δ and Bu together influence the physical- and spectral-space characteristics of internal scales and flow structure.

2. Equations of motion and the regime of linear potential vorticity

We consider the forced Boussinesq equations in a reference frame rotating about the vertical \hat{z} -direction [36–38], given by

$$\begin{aligned} \frac{D}{Dt} \mathbf{u} + f \hat{z} \times \mathbf{u} + \frac{1}{\rho_0} \nabla p + \frac{\rho}{\rho_0} g \hat{z} &= \nu \nabla^2 \mathbf{u} + \mathbf{f}_u \\ \frac{D}{Dt} \rho - b(\mathbf{u} \cdot \hat{z}) &= \kappa \nabla^2 \rho + \mathbf{f}_\rho, \quad \nabla \cdot \mathbf{u} = 0, \end{aligned} \quad (1)$$

where the Coriolis parameter $f = 2\Omega$ and Ω is the frame rotation rate. As usual, $D/Dt = \partial/\partial t + \mathbf{u} \cdot \nabla$ is the derivative following fluid particles, and the dynamical variables are the fluctuating part of the density $\rho(\mathbf{x}, t)$, the three-dimensional fluid velocity $\mathbf{u}(\mathbf{x}, t)$ with components (u, v, w) and the effective pressure $p(\mathbf{x}, t)$. The background stratification is linear and aligned with the rotation axis such that the total density is $\rho_T(\mathbf{x}, t) = \rho_0 - bz + \rho(\mathbf{x}, t)$. The dimensional coefficients ρ_0 and b

are positive constants, with b positive for stable stratification. Assumptions underlying the Boussinesq approximation are $|\rho| \ll \rho_0$ and $|\rho| \ll |bz|$ with background in hydrostatic balance $\rho_0 g = \partial p_0 / \partial z$. For some geophysical flows, it is more appropriate to expand around a background potential temperature instead of density [39]; modulo sign/coefficient changes, the basic structure of the equations remains the same. An inverse time scale characterizing the strength of the stratification is the buoyancy frequency $N = (gb/\rho_0)^{1/2}$ where g is the acceleration of gravity. The kinematic viscosity ν and the thermal diffusivity κ are associated with molecular processes.

All simulations will be done in a periodic domain, with constant f and N . Our investigation addresses the forward transfer of energy in (1) under the influence of a large-scale, random force $\mathbf{f}_u, \mathbf{f}_\rho$. The domain will have unit aspect-ratio or small aspect-ratio, with vertical domain height H_d and horizontal domain length L_d such that $H_d/L_d = \delta \leq 1$. The external force $\mathbf{f}_u, \mathbf{f}_\rho$ is localized in wavenumber, with peak forcing wavelength $H_f = H_d/4$ held fixed at one-quarter of the domain height.

In a rectilinear domain with dimensions (L_d, L_d, H_d) , an appropriate non-dimensionalization of (1) scales vertical distances z by $H = 2\pi/k_f$ where k_f is the peak wavenumber of the forcing, and horizontal distances x and y by $L = H/\delta$. For a forcing \mathbf{f}_u which projects equally onto horizontal and vertical components of velocity, all velocity components are scaled by the same characteristic large-scale velocity $U = (\varepsilon/k_f)^{1/3}$, where the force has energy input rate ε . Pressure is scaled by $\rho_0 U^2$ and density fluctuations by $B\rho_0$ with B (non-dimensional) constant. With time scaled by L/U , the non-dimensional form of (1) is given by

$$\begin{aligned} \frac{D_\delta}{Dt} \mathbf{u} + Ro^{-1} \hat{\mathbf{z}} \times \mathbf{u} + \nabla_\delta p + \gamma \rho \hat{\mathbf{z}} &= Re^{-1} \nabla_\delta \cdot \nabla_\delta \mathbf{u}, \\ \frac{D_\delta}{Dt} \rho - \gamma^{-1} (Fr \delta)^{-2} \rho w &= (Pr Re)^{-1} \nabla_\delta \cdot \nabla_\delta \rho, \quad \nabla_\delta \cdot \mathbf{u} = 0 \end{aligned} \quad (2)$$

where $D_\delta/Dt = \partial_t + \mathbf{u} \cdot \nabla_\delta$, $\nabla_\delta = \nabla_h + \hat{\mathbf{z}} \delta^{-1} \partial_z$, $\nabla_h = \hat{\mathbf{x}} \partial_x + \hat{\mathbf{y}} \partial_y$ and ∂_i is the partial derivative with respect to the position vector component x, y or z indexed by $i = 1, 2$ and 3 respectively. The Rossby and Froude numbers are here defined, respectively, by $Ro = U/(fL)$ and $Fr = U/(NH)$. Additional non-dimensional parameters are the aspect-ratio $\delta = H/L = H_d/L_d$ and $\gamma = BgL/U^2$, with constraint $\gamma = (\delta Fr)^{-1}$ for conservation of energy. The latter constraint selects the appropriate non-dimensional coefficient B in terms of the characteristic (imposed) velocity U by the consistency relation $B = U(g\rho_0/b)^{-1/2}$. The Reynolds Re and Prandtl Pr numbers defined for normal viscosity $Re = UL/\nu$, $Pr = \nu/\kappa$ could be replaced by analogous expressions involving hyper-coefficients, but these would not have any physical interpretation so we do not introduce them here.

For an unbounded or periodic domain, the linear eigenmodes of (2) are Fourier modes $[\mathbf{u}(\mathbf{x}, t; \mathbf{k}), \rho(\mathbf{x}, t; \mathbf{k})]^T = \phi^m(\mathbf{k}) \exp[i(\mathbf{k} \cdot \mathbf{x} - \sigma_m(\mathbf{k})t)]$ with four-component orthogonal basis vectors $\phi^m(\mathbf{k})$ (see, e.g., [9, 25] for explicit expressions for $\phi^m(\mathbf{k})$). There are three types of eigenmodes corresponding to $m = 0, \pm 1$. The $m = 0$ modes are usually called vortical modes $\phi^0(\mathbf{k})$ and have zero frequency $\sigma_0(\mathbf{k}) = 0$. The $m = \pm 1$ modes are two wave modes $\phi^\pm(\mathbf{k})$ with frequency $\sigma_\pm(\mathbf{k})$ given by the dispersion relation

$$\sigma_\pm(\mathbf{k}) = \pm \frac{(Fr^{-2} k_h^2 + Ro^{-2} k_z^2)^{1/2}}{(k_h^2 \delta^2 + k_z^2)^{1/2}}, \quad (3)$$

where $k_h = (k_x^2 + k_y^2)^{1/2}$ is the horizontal wavenumber. The slowest wave modes with $k_h = 0$ and frequency $\sigma_{\pm} = \pm Ro^{-1}$ correspond to VSHF, with zero vertical velocity and zero vertical vorticity. The linear eigenmodes serve as a useful orthogonal and complete basis to represent the solution to the full nonlinear equations:

$$[\mathbf{u}(\mathbf{x}, t), \rho(\mathbf{x}, t)]^T = \sum_{\mathbf{k}} \sum_{m=0, \pm} b_m(\mathbf{k}, t) \phi^m(\mathbf{k}) \exp[i(\mathbf{k} \cdot \mathbf{x} - \sigma_m(\mathbf{k})t)] \quad (4)$$

where the amplitudes $b_m(\mathbf{k}, t)$ are now the unknowns to be determined [9, 33].

The vortical and wave-mode decomposition is a natural way to expose the dynamical hierarchy in terms of resonant, near-resonant and non-resonant interactions that results from the dispersive modulation of the advective nonlinearity (see [9, 37, 40, 41] for details of the wave-vortical decomposition). Indeed, much of our understanding of rotating and stratified turbulence is based on the wave-vortical mode decomposition. Exact resonances are interactions that satisfy the triad condition $\mathbf{k} + \mathbf{p} + \mathbf{q} = 0$ and the resonance condition $\sigma(\mathbf{k}) + \sigma(\mathbf{p}) + \sigma(\mathbf{q}) = 0$, and they appear at next-to-lowest order in a formal perturbation expansion of the Fourier-transformed equations (2) about the Rossby and/or Froude number(s). As the name suggests, near-resonant interactions appearing at higher order satisfy the resonance condition only up to an error of $O(Fr)$ or $O(Ro)$. As the Rossby and/or Froude numbers approach zero, some or all of the exact resonances dominate the dynamics. For $Ro \sim Fr = \epsilon \rightarrow 0$, exact resonances between vortical modes dominate, with $\sigma_0(\mathbf{k}) + \sigma_0(\mathbf{p}) + \sigma_0(\mathbf{q}) = 0$. The well-known quasi-geostrophic (QG) approximation is associated with interactions among vortical modes [9, 25, 28, 40], and different derivations of the quasi-geostrophic equations include the original scaling analysis [5, 24], a mathematically rigorous averaging procedure [25], analysis of small divisors [1, 28], and a formal non-perturbative reduction [9, 42]. The limit $Fr \rightarrow 0$ with $Ro = \mathcal{O}(1)$ or infinity has also been analyzed from different points of view [1, 3, 5, 25]. Of note are at least two important differences compared to $Fr \sim Ro \rightarrow 0$: (i) three-wave exact resonances are non-negligible, with $\sigma_{\pm}(\mathbf{k}) + \sigma_{\pm}(\mathbf{p}) + \sigma_{\pm}(\mathbf{q}) = 0$, (ii) the VSHF persist in time as shown rigorously by [25]. Although it is known that exact resonances cannot transfer energy to VSHF modes, the studies [9, 19] for finite, small Fr indicate that near-resonant, three-wave interactions are primarily responsible for the generation of VSHF. Some theoretical analyses account explicitly for small-aspect-ratio domains [1, 5]. In particular, [1] showed that near-resonant, three-wave interactions are sparse for small-aspect-ratio, $Fr \rightarrow 0$, $Bu = \mathcal{O}(1)$ flows.

Foundational laws for rotating, stratified fluids in the inviscid, non-diffusive limit are (i) conservation of energy, and (ii) conservation of potential vorticity following fluid particles [23]. Global energy conservation is given by

$$\partial_t E = \partial_t \int_D E(\mathbf{x}) d\mathbf{x} = \partial_t \int_D \frac{1}{2}(\mathbf{u} \cdot \mathbf{u} + \rho^2) d\mathbf{x} = 0 \quad (5)$$

where \int_D indicates integration over the domain. The potential vorticity q is defined as $q = (\boldsymbol{\omega} + Ro^{-1}\hat{\mathbf{z}}) \cdot \nabla_{\delta}\rho_T$, and its derivative following fluid particles vanishes according to

$$\begin{aligned} \frac{D_\delta}{Dt} q = \frac{D_\delta}{Dt} \left((Ro \delta)^{-1} \partial_z \rho - (Fr \delta)^{-1} \boldsymbol{\omega} \cdot \hat{\mathbf{z}} + \delta^{-1} (\partial_z u \partial_y \rho - \partial_z v \partial_x \rho + (\boldsymbol{\omega} \cdot \hat{\mathbf{z}}) \partial_z \rho) \right. \\ \left. + (\partial_y w \partial_x \rho - \partial_x w \partial_y \rho) \right) = 0, \end{aligned} \quad (6)$$

where $\boldsymbol{\omega}$ is the relative vorticity $\boldsymbol{\omega} = \nabla_\delta \times \mathbf{u}$. The constant piece of q (that is, $Ro^{-1} Fr^{-1} \delta^{-1}$) has been dropped since it does not contribute to the conservation law (6). While energy conservation (5) does not depend on any of the salient non-dimensional parameters, the conservation of potential vorticity (6) does. Therefore it is useful to use potential vorticity to define our parameter space and to differentiate this work from related work.

The linear piece of (6), $q_{lin} = (Ro \delta)^{-1} \partial_z \rho - (Fr \delta)^{-1} \boldsymbol{\omega} \cdot \hat{\mathbf{z}}$, is the pseudo-potential vorticity conserved by the QG equations. One series of flows simulations has $\delta = 1$ with fixed small Fr , and Ro varying from $Ro = Fr$ to $Ro \simeq \mathcal{O}(10^{-1})$. This series of runs has linear potential vorticity $\simeq (Ro \delta)^{-1} \boldsymbol{\omega} \cdot \hat{\mathbf{z}} + (Fr \delta)^{-1} \partial_z \rho$, (both Ro and Fr dependencies are significant) or $\simeq (Fr \delta)^{-1} \partial_z \rho$ (for the case where $Ro \simeq \mathcal{O}(10^{-1})$), with all other terms being subdominant. The second series of flow simulations has decreasing δ and $Ro = Fr$ (fixed small). In this case, the potential vorticity is again linear and dominated by the sum $(Ro \delta)^{-1} \boldsymbol{\omega} \cdot \hat{\mathbf{z}} + (Fr \delta)^{-1} \partial_z \rho$.

Our chosen parameter regimes might be contrasted with studies of purely stratified small aspect-ratio flows [17, 35, 43] ($Ro \rightarrow \infty$) and with vertical Fr relatively large. Indeed [35] first indicated that the Nastrom-Gage spectrum parameter regimes might be associated with non-linear potential vorticity. The numerical simulations of stratified flows by [17] directly address the parameter regime thought to be of interest for the Nastrom-Gage spectrum [34]. In that study, it was shown that the scales need to be resolved well past the buoyancy scale $L_b = 2\pi U/N$ down to the Ozmidov scale L_O (the outer scale of turbulence), in order to obtain converged spectra with the dual scaling regime thought to be typical of the atmospheric mesoscales. By contrast, our aim in this study is to both include the effects of rotation and aspect-ratio, and to minimize nonlinear potential vorticity contributions to understand some of the leading-order qualitative and quantitative aspects of structure formation in a fairly well-controlled parameter sub-space. This choice necessarily leads to a set of simulations for which L_b is marginally resolved at best (see Table 1). Thus, in our simulations there is no overturning due to wave dynamics. We also do not resolve scales larger than the forcing scale, and the focus of our study is a range of scales smaller than the forcing scale, but larger than L_b .

The buoyancy Reynolds number $R_B \simeq Re(Fr/\delta)^2$, where $Re = UL/\nu$ is the Reynolds number based on a characteristic horizontal scale, is useful to characterize the competing influences of turbulence and stratification. The importance of R_B in the transition from viscous dominated to stratification domination flows was first discussed in [14]. Following those arguments, [20] explored the relationship between the R_B and the quadratic potential enstrophy (one-half the square of the potential vorticity) in the context of atmospheric flows. It was shown that for flows with $R_B > 1$, the potential enstrophy is quartic while for flows with $R_B < 1$, the potential enstrophy is quadratic. Since atmospheric flows are estimated to have $R_B \gg 1$, the author concludes that quartic potential enstrophy is quite likely to characterize such flows thus rendering the quadratic potential enstrophy condition less critical to atmospheric flows.

Although the standard Reynolds number is not well-defined in our flows due to the use of hyperviscosity, our extremely small Fr likely places our flows in the

regime of $Re_B < 1$, consistent with quadratic potential enstrophy according to [20]. Given the theoretical inclination of our studies we propose quadratic potential enstrophy as a well-defined limit for detailed parameter studies tied closely with rigorous theory. Laboratory experiments also tend to be in the $Re_B \ll 1$ regime due to the difficulty of achieving extremely high Reynolds numbers [21, 22]. Furthermore, a better understanding of such asymptotic regimes might yield useful benchmarks and test-beds for model validation.

Since the potential vorticity q is a sign indefinite quantity, we use the potential enstrophy as a surrogate to monitor development of q [33]. The total potential enstrophy is defined as

$$Q = \frac{1}{2} \int_D q^2 d\mathbf{x}, \quad (7)$$

and its quadratic part

$$Q_{\text{quad}} \equiv \frac{1}{2} \int_D \delta^{-2} (Ro^{-1} \partial_z \rho - Fr^{-1} \boldsymbol{\omega} \cdot \hat{\mathbf{z}})^2 d\mathbf{x}. \quad (8)$$

will dominate when $q \sim q_{\text{lin}}$. The scan of the parameter space in what follows will be accomplished by tracking the potential enstrophy.

3. Numerical Simulations

Pseudo-spectral calculations of the Boussinesq equations with rotation are performed on domains with aspect-ratio $\delta = H_d/L_d \leq 1$, dimensions $L_d \times L_d \times H_d = 1 \times 1 \times \delta$ and $N_x \times N_y \times N_z$ gridpoints. Requiring isotropic grids, we have $N_x = N_y = N_z/\delta$. Fourth-order Runge-Kutta time-stepping is used, the inertia-gravity wave frequencies are adequately resolved. An eighth-order hyperviscosity/diffusion $(\nabla^2)^8$ is used in place of ∇^2 in both the momentum and density equations following what has become standard practice to extend the inertial range of scales. Therefore the viscous/diffusion constants ν and κ used in practice are not physical. As discussed in the Introduction, our work focusses on the range of scales characterized by linear potential vorticity; those scales are larger than the buoyancy scale and well-removed from the dissipation scale. Hence for the scales of interest here, we expect the effects of hyperviscosity/diffusion to be sub-dominant.

The rate of energy input in all cases is fixed at $\epsilon_f \approx 1$. The forcing is chosen to peak at the fourth wavenumber shell $k_f = 4 \times \Delta k$, namely at scales one-quarter of the height of the domain. Both wave and vortical modes are equally forced at each forced wavenumber. Identical forcing schemes were used in [31, 33] where further details are available.

The fourier modes are dealiased using the 2/3-rule giving an effective small-scale grid of $\Delta x \times \Delta y \times \Delta z = 1.5/N_x \times 1.5/N_y \times 1.5 \delta/N_z$. The wavenumber in the horizontal $k_h = (k_x^2 + k_y^2)^{1/2}$ has increments $\Delta k_h = 2\pi/L_d = 2\pi$ while the vertical wavenumber has increments $\Delta k_z = 2\pi/H_d = 2\pi/\delta$. The spherical increment (shell thickness) is defined using the vertical wavenumber increments $\Delta k = \Delta k_z$.

Based on the characteristic forcing velocity scale $U = (\epsilon_f/k_f)^{1/3}$, vertical scale $H = 2\pi/k_f$ and horizontal scale $L = H/\delta$, the $Fr = U/(NH)$, and $Ro = U/(fL)$. The values of N are chosen to (approximately) fix $Fr \simeq 0.002$ in all cases. At this value of Fr , we know that all the flows are in the regime of quadratic potential enstrophy (see Figure 1). The buoyancy scale $L_b = 2\pi U/N$ is under-resolved with $\Delta x/L_b$ ranging from 4 to 23 (see Table 1). The smallest aspect-ratio flow is the least

resolved with respect to L_b due to our decision to fix Fr so as to be able to compare across a wide range of flows. In order to fix Fr at fixed resolution, as δ decreases and the forcing wavelength remains fixed at one-quarter the domain height, the value of N required is unavoidably high, hence the very small L_b . We proceed to study layer formation in the scales larger than L_b across a wide parameter range.

run	grid	$\delta = H_d/L_d$	Ro	Fr	Bu	N/f	$\Delta x/L_b$
B1	$640 \times 640 \times 640$	1	0.0023	0.0023	1	1	4.08
B4	$640 \times 640 \times 640$	1	0.0091	0.0023	4	4	4.07
B8	$512 \times 512 \times 512$	1	0.016	0.002	8	8	5.85
B16	$512 \times 512 \times 512$	1	0.032	0.002	16	16	5.85
B32	$512 \times 512 \times 512$	1	0.064	0.002	32	32	5.85
d4	$2048 \times 2048 \times 512$	0.25	0.002	0.002	1	4	5.85
d8	$2048 \times 2048 \times 256$	0.125	0.002	0.002	1	8	11.7
d16	$2048 \times 2048 \times 128$	0.0625	0.002	0.002	1	16	23.43

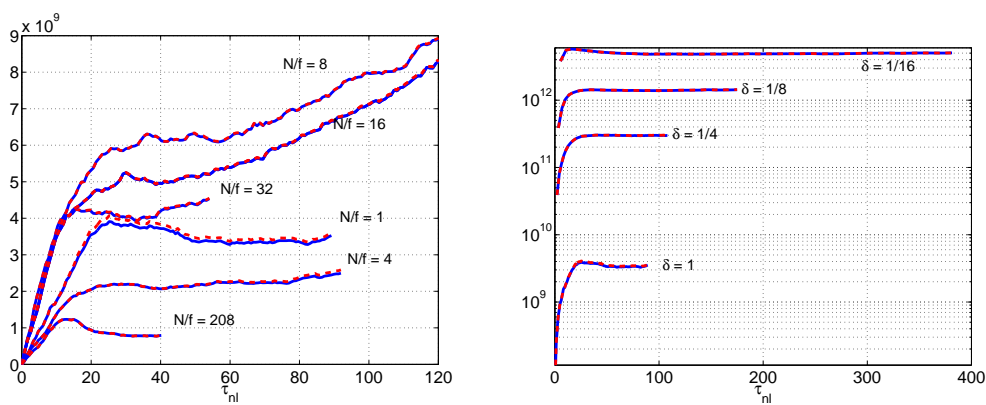
Table 1. Parameters of the numerical simulations of the Boussinesq equations.

The first set of flows is denoted by prefix ‘B’, since Bu is varied at fixed unit aspect-ratio (Table 1). We fix $Fr = Fr_o \simeq 0.002$, $\delta = 1$ and vary Ro such that $Bu = Ro/Fr = 1, 4, 8, 16$ and 32 . This provides for a study of layer formation strictly as a function of Ro for fixed Fr . The second set of flows is denoted by prefix ‘d’, since the aspect-ratio δ is varied at fixed $Bu = 1$. Again fixing $Fr = Fr_o = 0.002$ and $Bu = \delta N/f = 1$, we choose $N/f = 4, 8$ and 16 to match (some of) the N/f values in the B-series; consequently setting $\delta = 1/4, 1/8$ and $1/16$ in d4, d8 and d16 respectively. We perform three comparative studies: B-series (effect of Ro for fixed $Fr_o \simeq 0.002$), d-series (effect of aspect-ratio for fixed $Bu = 1$ and fixed $Fr_o \simeq 0.002$) and between the B- and d-series (effect of changing δ from 1 to f/N for fixed N/f). There are, of course, numerous other parameter variations that could have been explored. We are providing a partial exploration into the myriad combinations of Ro , Fr , Bu , N/f and δ that are possible in such flows, with a specific focus on the variability of structure (layer) formation.

The nonlinear timescale based on the forcing scale $\tau = (\epsilon_f k_f^2)^{-1/3}$ is used to non-dimensionalize time t such that $\tau_{nl} = t/\tau$. Figure 1 shows the evolution of potential enstrophy and of its quadratic component for both sets of flows as a function of τ_{nl} . By this measure it is clear that all flows are in the quadratic potential enstrophy regime which provides a reasonably well-defined limiting regime in the parameter space wherein (potentially uncontrolled) nonlinear potential vorticity effects are not a factor. Note that Fig. 1(a) shows potential enstrophy of the $Bu > 1$ flows growing in time, indicating that at least a part of the potential enstrophy is transferred upscale of the forcing where there is no dissipative mechanism. In Fig. 1(b), all the flows have $Ro = Fr$ and the potential enstrophy saturates rather quickly in time suggesting that all the potential enstrophy transfers downscale and is dissipated in the small scales.

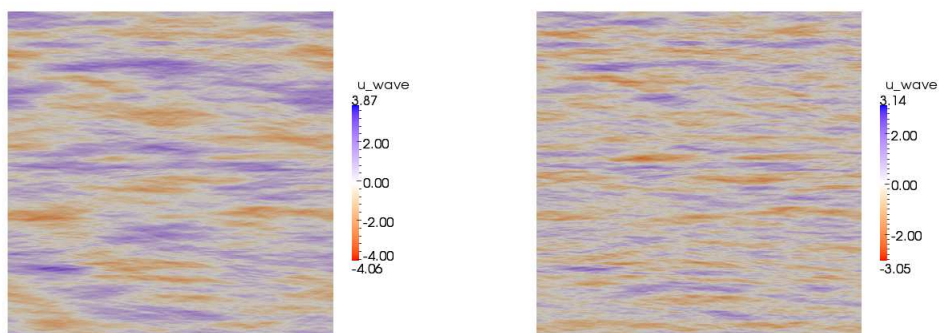
3.1. B-series comparison: fixing $\delta = 1$, $Fr \simeq 0.002$, varying Ro

We begin with a comparison of unit aspect-ratio flows B1-B32, which have (nearly) fixed $Fr = Fr_o$, identical forcing, and comparable resolution of the buoyancy scale $4 < \delta x/L_b < 5.8$ (that is, nearly constant N). The Coriolis parameter f is varied so that N/f increases from 1 to 32. Effectively, Ro is increased from 0.002 to 0.064 in this series. The structure of the flow is visualized using the wave and vortical



(a) B-series: $\delta = 1$ flows for fixed $Fr \simeq 0.002$, Ro/Fr increasing from 1. (b) d-series: $Bu = 1$ flows for fixed $Fr \simeq 0.002$, decreasing δ (increasing N/f). Note that the y -axis is logarithmic for clarity.

Figure 1. Global potential entrophy Q (solid line) and its quadratic component Q_{quad} (dashed-line) for all the flows in the database, as a function of non-dimensional time. The two lines practically coincide in all cases, indicating that flows are in the asymptotically quadratic potential entrophy regime by this measure.



(a) Surface contours of the wave component of u for B4. (b) Surface contours of the wave component of u for B4 with only $k > 5$ modes retained.

Figure 2. Two visualizations of B4 using the wave-component of u .

components of u , the x -component of the velocity \mathbf{u} . From Eq. (4) we have

$$u^\pm(\mathbf{x}, t) = \sum_{\mathbf{k}} \sum_{m=\pm} b_m(\mathbf{k}) \phi_1^m(\mathbf{k}) \exp[i(\mathbf{k} \cdot \mathbf{x} - \sigma_m(\mathbf{k})t)] \quad (9)$$

$$u^0(\mathbf{x}, t) = \sum_{\mathbf{k}} b_0(\mathbf{k}) \phi_1^0(\mathbf{k}) \exp[i(\mathbf{k} \cdot \mathbf{x} - \sigma_m(\mathbf{k})t)] \quad (10)$$

Similar projections may be defined for v , w and ρ . density. Figure 2(a) shows surface contours of u^\pm at the latest time for flow B4 with evident layered structure. The signature of the forcing is apparent in the unfiltered flow in the form of larger coherent structures. In Fig. 2(b) we show the same flow field with modes $k < 5$ filtered out. It is clear from the filtered version that the layering persists to much smaller scales than the characteristic large and forced scales. The vortical component of the velocity visualized in this way (not shown) also shows the signature of the forcing. In order to avoid biasing the eye to the forcing signature, in the development of structure in the sub-forcing scales, in subsequent visualization we show fields for which the low modes ($k < 5$) have been filtered out. However our spectra and scale calculations presented later in the paper retain all modes.

3.2. Equal time data-analysis

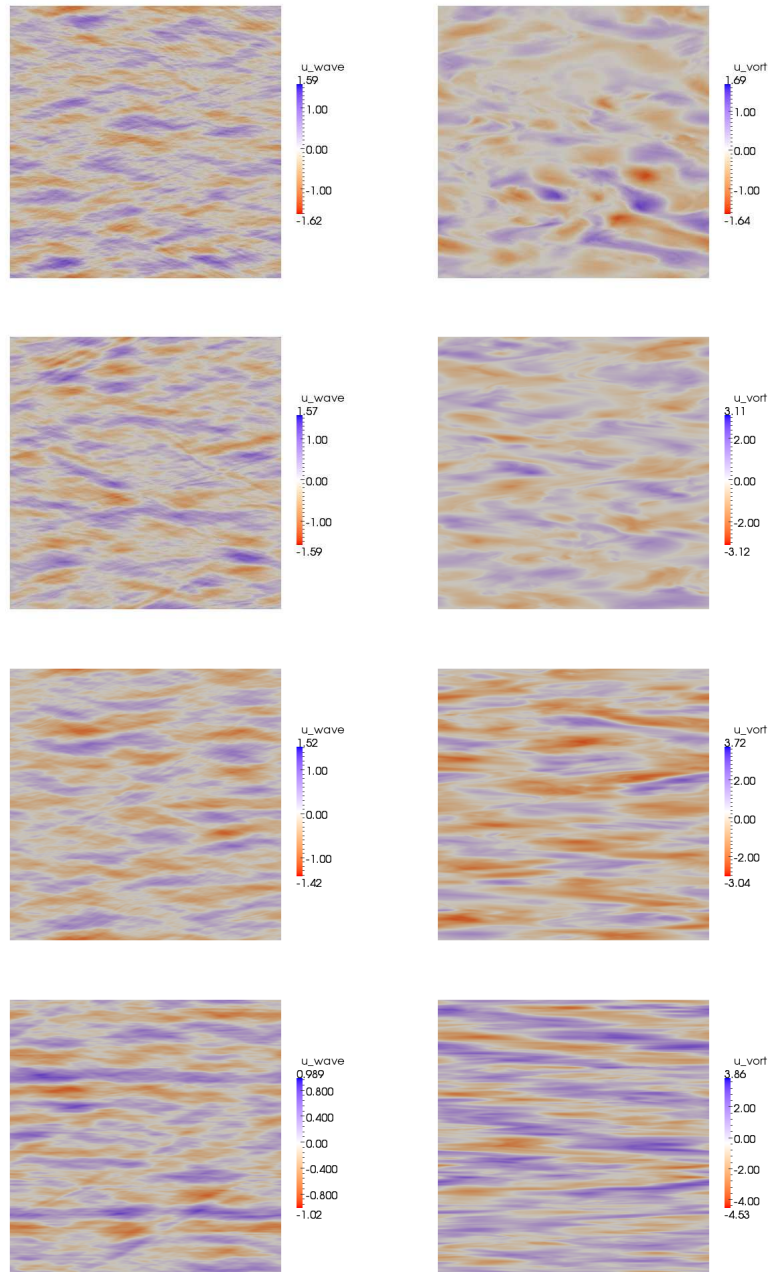


Figure 3. Visualization of a $(y-z)$ slice of the u field at $\tau_{nl} \simeq 50$ for the $\delta = 1$ (B-series) simulations for the wave (left column) and vortical (right column) component of u . From top (for $Fr_o \simeq 0.002$): ($Ro = 0.0091, N/f = 4$) (B4), ($Ro = 0.016, N/f = 8$) (B8), ($Ro = 0.032, N/f = 16$) (B16), ($Ro = 0.064, N/f = 32$) (B32). The wavenumbers $k \leq 5$ have been filtered out in all cases in order to focus on sub-forcing scales.

Since our flows are run out to different non-linear times (see Fig. 1) we first compare B4-B32 at equal time $\tau_{nl} \simeq 50$ (the latest time for B32). Layered structure has emerged in the wave modes in all four cases (left column Fig. 3). The vortical component shows very weak structures for B4, becoming more distinct for higher values of Ro (B8, B16, B32, right column Fig. 3). From these early time visualizations we may conclude qualitatively, that: a) layering is set up at early times in all cases, b) for relatively small N/f ($Ro \simeq 4Fr_o$) the layers observed in

the vortical component of the flow are not very distinct, and the magnitude of the vortical and wave components are comparable, c) for larger N/f ($Ro \geq 8Fr_o$) the layered structure become more distinct in the vortical mode and the magnitude of the vortical component becomes much larger than the wave component, and d) fine scale layered structure in the vertical increases in the wave component as Ro increases, but the magnitude of the wave component is becomes subdominant to the vortical.

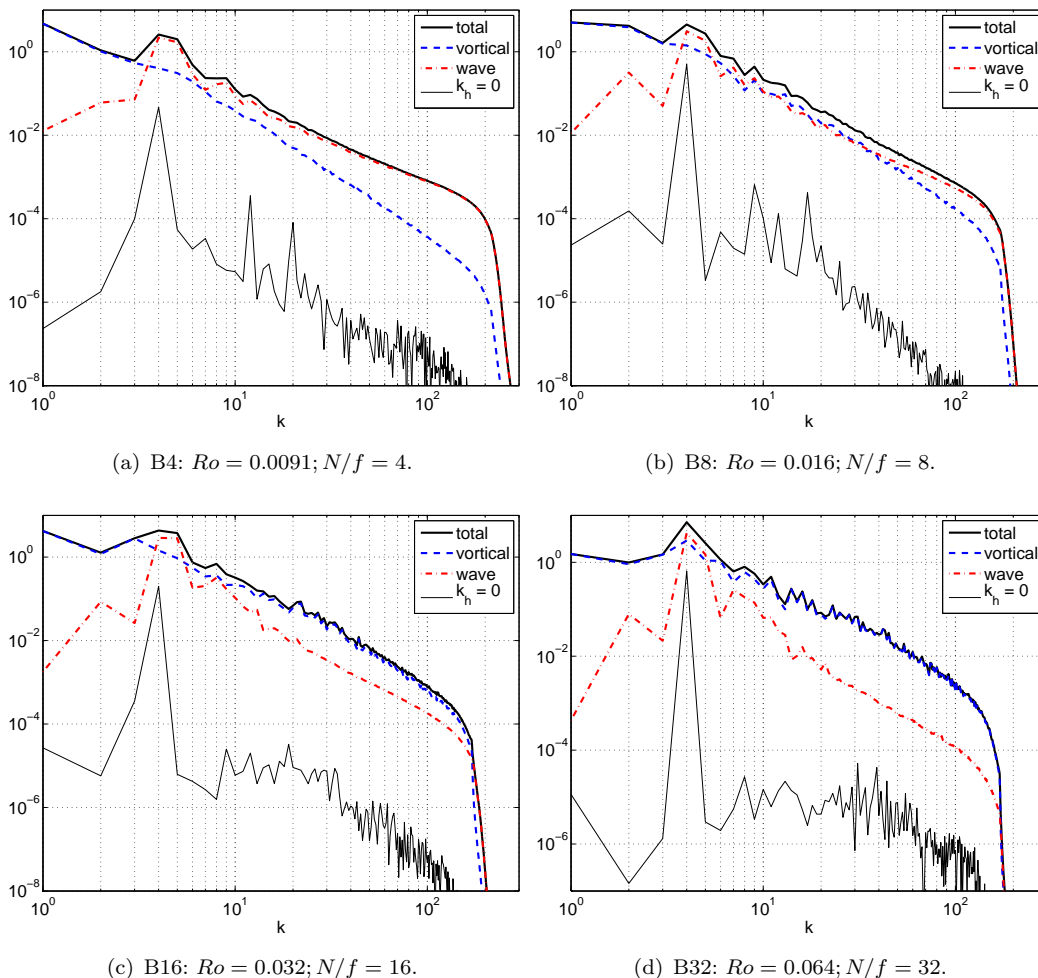


Figure 4. Wave, vortical and $k_h = 0$ (wave) mode spectra for B-series $\delta = 1, Fr \simeq 0.002$ flows with $(Ro, N/f)$ as indicated, at $\tau_{nl} = 50$ nonlinear times. The VSHF (excluding the forcing scales) are not significant at these early times.

The wave and vortical energy spectra as a function of wavenumber k for a given time t are defined as:

$$\begin{aligned}
 E^\pm(k, t) &= \frac{1}{2} \sum_{(\Delta k)_s} \Delta k (|b^+(\mathbf{k}, t)|^2 + |b^-(\mathbf{k}, t)|^2) \\
 E^0(k, t) &= \frac{1}{2} \sum_{(\Delta k)_s} \Delta k |b^0(\mathbf{k}, t)|^2
 \end{aligned} \tag{11}$$

where $\sum_{(\Delta k)_s}$ indicates summation over all wavenumbers $k - \frac{1}{2}\Delta k < |\mathbf{k}| \leq k + \frac{1}{2}\Delta k$ within the shell of thickness Δk . The wave and vortical energy spectra as defined

above are shown in Fig. 4 for equal time $\tau_{nl} = 50$. For B4 the vortical energy scales as k^{-3} , nominally characteristic of quasi-geostrophic flow [24]; both the vortical-mode energy and the VSHF energy are subdominant to the wave-mode energy for wavenumbers $k > k_f$. As Ro increases (B8) the vortical energy becomes comparable to the wave energy with scaling shallower than k^{-3} in a wide intermediate range of scales. As Ro increases even further (B16 and B32), the vortical contribution dominates the total energy. In summary, the VSHF are unimportant at these (early) times, and a transition from wave-mode dominance to vortical-mode dominance with respect to energy distribution is observed as Ro increases. This is consistent with the visualizations (Fig. 3) in which vortical mode shows increasing fine structure in the vertical and wave-mode amplitudes decrease as Ro increases.

3.3. Late time data-analysis

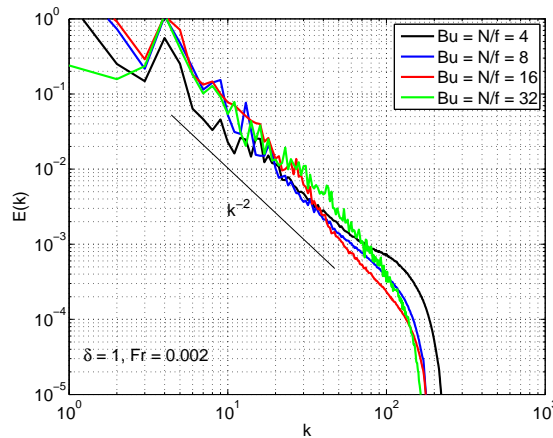


Figure 5. Comparison of the total energy spectra for all flows in the B-series. The k^{-2} line is placed only as a reference scaling.

We observe that the (latest time) *total* energy spectra of each of the flows in the B-series (Fig. 5) are more or less comparable. A k^{-2} scaling line is shown as a guide to the eye. Indeed a precise scaling exponent may not be an appropriate measure, with noisy intermediate scales emerging near the forcing scales and then at smaller wavenumbers, as Bu increases. However the overall decay trend seems close to k^{-2} , distinct both from k^{-1} expected for the wave component and from k^{-3} expected for the vortical component in quasi-geostrophic flow. The similarity in shape and magnitude of the total energy spectrum for all the B-series flows provides further support to the notion that differences between them become clear only in a deeper dissection such as the wave-vortical mode decomposition.

In Fig. 6 we compare visualizations of B1 through B16 (the latest-time of the B32 flow was presented in the previous section) at the latest simulation time for each flow. As expected, for $Ro = Fr$ (B1) there is an absence of layering. For B4-B16, the visualizations are consistent with early times – wave component layers are strongly evident in all cases, while as Ro increases from (B4, $N/f = 4$) to (B8, $N/f = 8$) the vortical component layers become more pronounced. We make the qualitative observation that the layers in the vortical mode display more fine-scale structure as Ro increases; the corresponding fine-scale structure of the wave-component decreases, consistent with the wave and vortical energy spectral trade-offs discussed below. Briefly, the visualization at the latest times show no real qualitative difference in the trends as Ro increases when compared to earlier times.

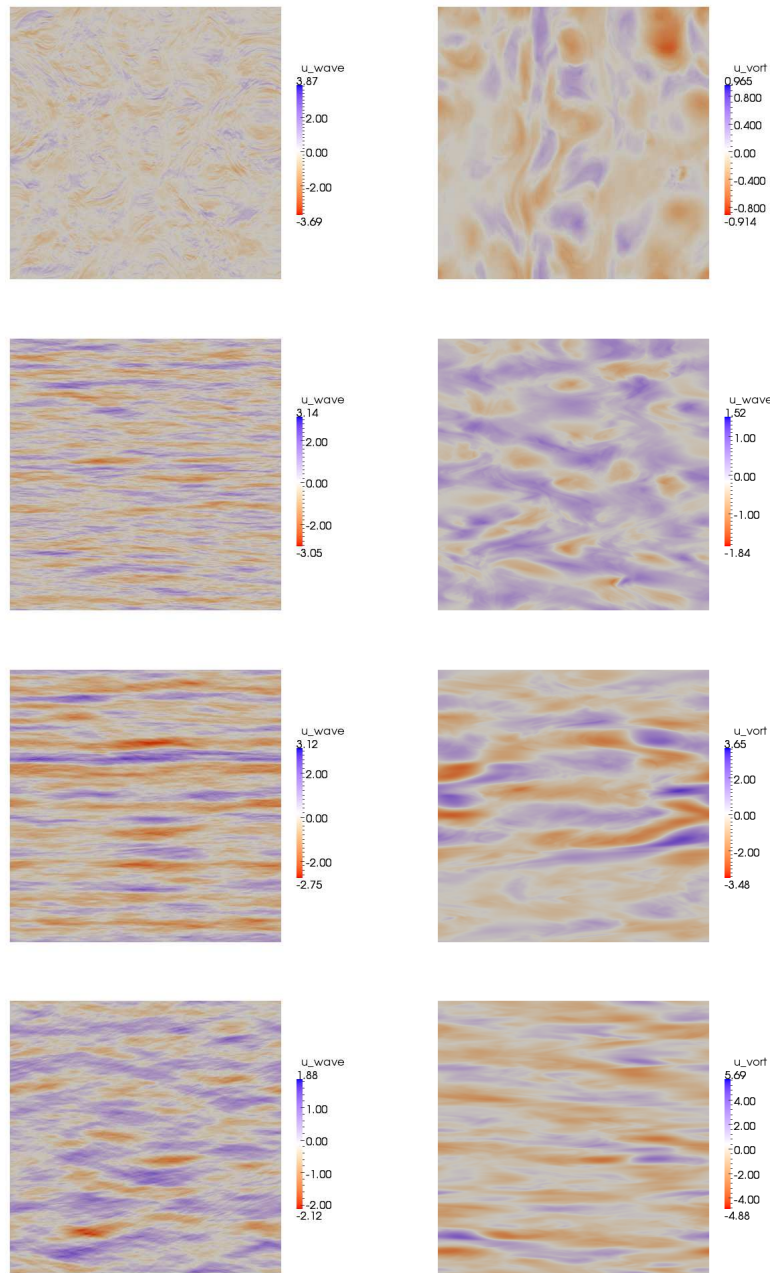


Figure 6. Visualization of a $(y-z)$ slice of the flow field at the latest time of the B-series of $(\delta = 1, Fr \simeq 0.002, N \simeq 4000)$ simulations showing iso-contours of the wave (left) and vortical (right) component of the horizontal velocity. From top: $(Ro = 0.00227, N/f = 1)$ (B1), $(Ro = 0.0091, N/f = 4)$ (B4), $(Ro = 0.016, N/f = 8)$ (B8), and $(Ro = 0.032, N/f = 16)$ (B16). The wavenumbers $k \leq 5$ have been filtered out in all cases in order to focus on sub-forcing scales.

In Fig. 7 we show the total energy, the wave energy, the vortical energy and the contribution to the wave energy from the VSHF, at the latest simulation time, for the B-series. Note that the latest time spectra for B32 is already given in Fig. 4. As is now well-known (see for example [40, 44]) the vortical energy goes from being subdominant in B4 ($N/f = 4$), to being comparable to the wave energy in B16 to being dominant in B32. For both B4 and B8, there is significant energy in the VSHF at these late times (to be contrasted with the lack of VSHF early time data). It is not possible to rule out the appearance of significant VSHF in the B16 and B32 flows if they were to be run to even longer times. Note that B4 was run

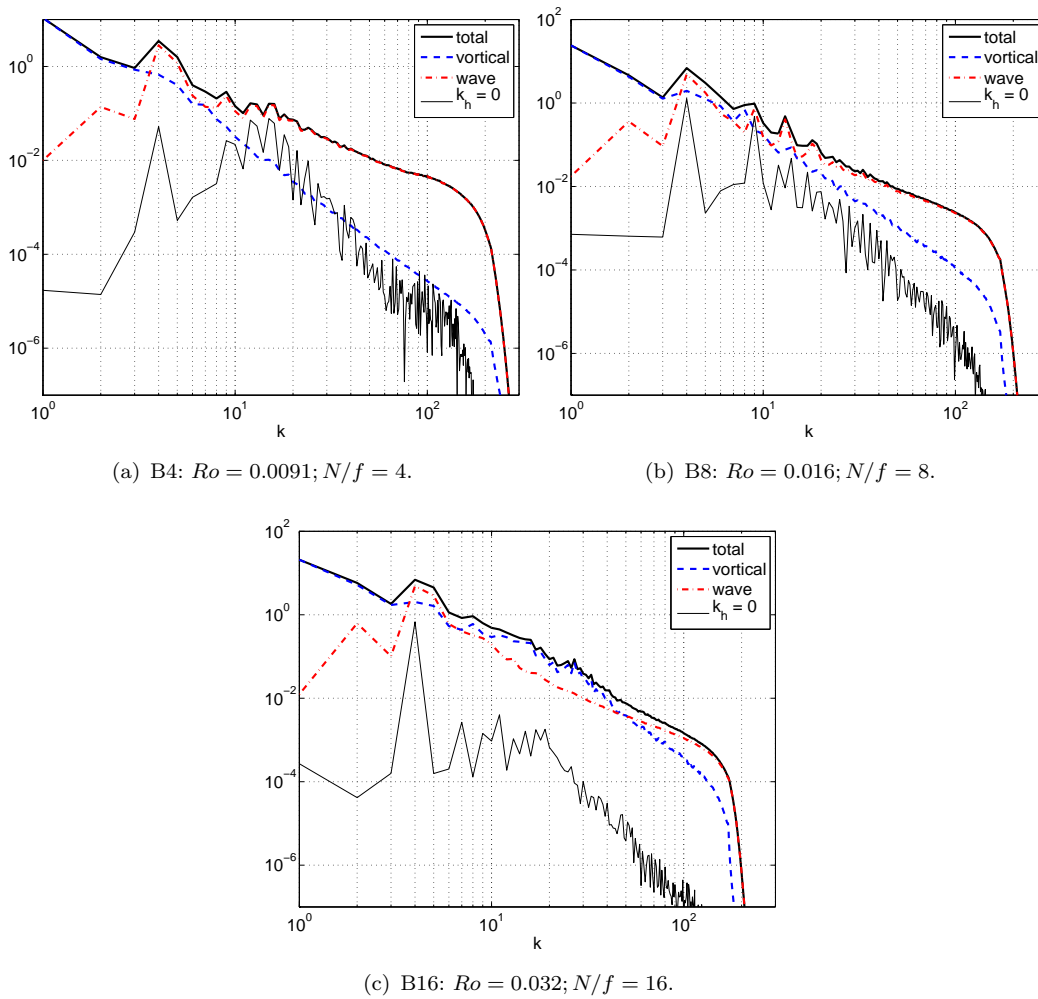


Figure 7. Wave, vortical and $k_h = 0$ (wave) mode spectra for B-series ($\delta = 1, Fr \simeq 0.002$) flows at their respective latest times. The VSHF (excluding the forcing scales) are significant only for $Ro = 0.0091$ ($N/f = 4$) and $Ro = 0.016$ ($N/f = 8$).

to $\tau = 90$ while *B8* and *B16* was run to $\tau_{nl} = 120$; and the first has the most pronounced VSHF. We may infer that for fixed small Fr , increasing Ro delays and, possibly, inhibits the appearance of VSHF in the small scales. It may also well be that the VSHF would appear in the large scales (low wavenumbers) after long times, if we had a substantial range of large scales resolved, similar to the simulations of [9]. This particular issue cannot be resolved without much longer runs for all cases which is not within our present capabilities.

Another representation of the layer formation may be seen in the increasing asymmetry of the wave and vortical energy spectra as a function of horizontal (k_h) and vertical (k_z) wavenumber components. These are defined as:

$$\begin{aligned}
 E^{\pm[0]}(k_h, t) &= \sum_{k_z} \Delta k_z \sum_{(\Delta k_h)_S} \Delta k_h E^{\pm[0]}(\kappa_h, k_z) \\
 E^{\pm[0]}(k_z, t) &= \sum_{k_h} \Delta k_h \sum_{(\Delta k_z)_S} \Delta k_z E^{\pm[0]}(k_h, \kappa_z)
 \end{aligned} \tag{12}$$

where $\sum_{(\Delta k_h)_S}$ indicates summation over all wavenumbers in the annulus

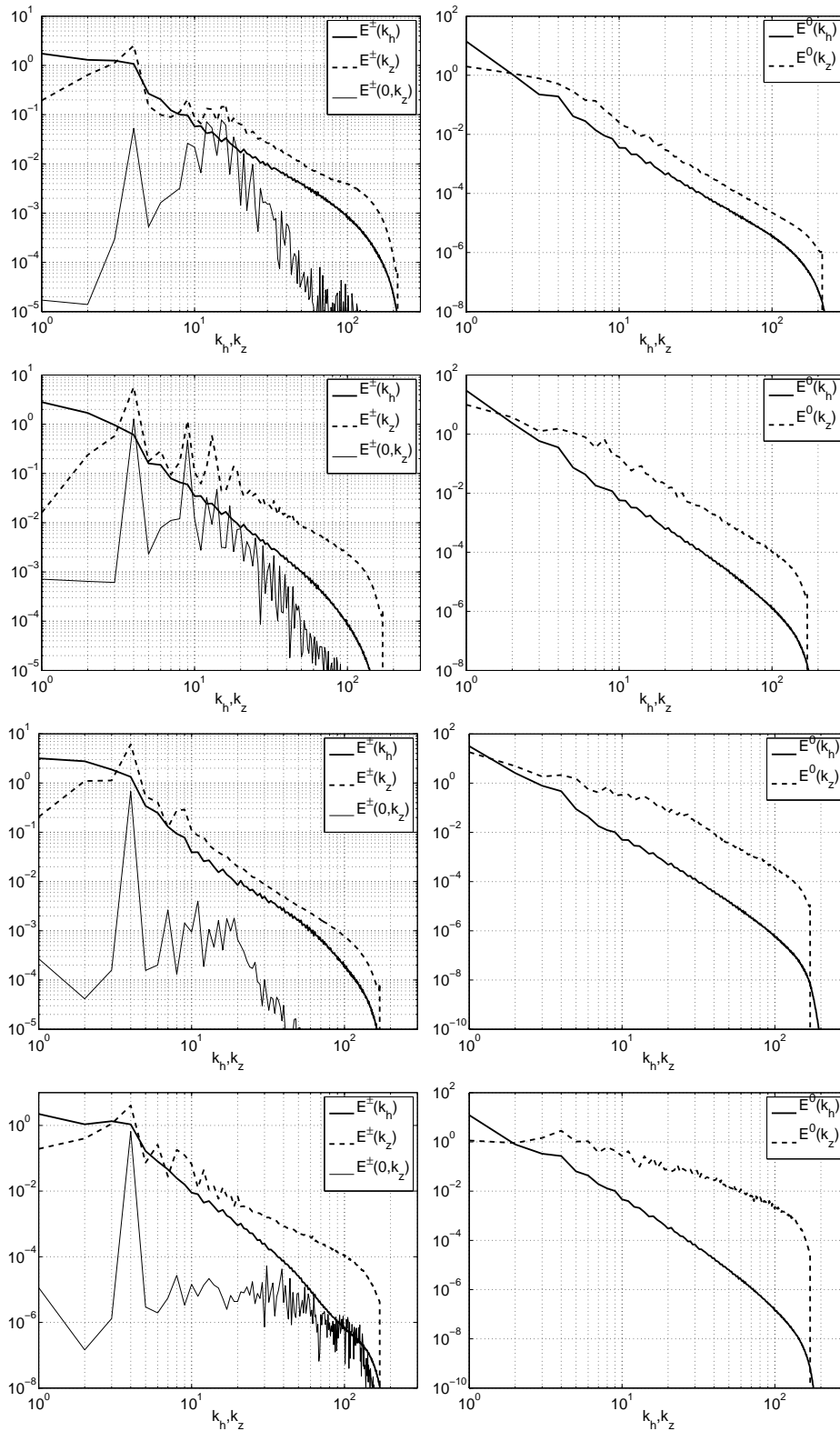


Figure 8. For the B-series ($\delta = 1, Fr \simeq 0.002$) flows, left column: wave energy as a function of k_h (summed over k_z), as a function of k_z (summed over k_h), and as a function of k_z for fixed $k_h = 0$ (VSHF); right column: vortical energy as a function of k_h and k_z . Top to bottom: ($Ro = 0.0091, N/f = 4$), ($Ro = 0.016, N/f = 8$), ($Ro = 0.032, N/f = 16$), ($Ro = 0.064, N/f = 32$).

$k_h - \frac{1}{2}\Delta k_h < k_h \leq k_h + \frac{1}{2}\Delta k_h$ and $\sum_{(\Delta k_z)_s}$ indicates summation over the wavenum-

bers on the line fraction $k_z - \frac{1}{2}\Delta k_z < k_z \leq k_z + \frac{1}{2}\Delta k_z$. In Fig. 8 we show that as Ro increases there is a marked difference in the rate of decay of $E^{\pm[0]}$ along k_h as compared to the decay along k_z . An increased accumulation in large k_z with rapid decay at large k_h is a characteristic signature for layers, indicating fine scale structure in the vertical. This is consistent with the observed layered structure, particularly for the vortical modes. The right column of Fig. 8 shows that, as Ro increases, the decay rate for $E^0(k_h)$ increases while $E^0(k_z)$ becomes increasingly flat. The wave energy spectra shows qualitatively similar behavior as Ro increases (left column of Fig. 12) but the asymmetry in the spectra for k_z vs k_h is not as strong, consistent with less fine structure of the wave-component in the vertical and perhaps less distortion (relative flattening) of the associated structures (consistent with the visualizations).

Our visualizations and results for energy spectra are consistent with previous work. For example, growth of the VSHF has been observed for stratification dominated flows by [9, 13, 19, 26]. For purely stratified flows and decreasing Fr [14, 26, 44] observed steepening of spectra with respect to horizontal wavenumber k_h and flattening spectra with respect to the vertical wavenumber k_z . In those simulation (without rotation and with different forcing) and in our spectra reported above such asymmetry is consistent with layering. Overturning is not resolved both in the simulations with $R_B < 1$ of [14, 26, 44] as well as in our B-series. In the following sections, we begin to systematically explore the impact of small aspect-ratio on both wave-mode and vortical-mode layer formation. We further attempt to quantify internal layer thicknesses in Section 4.

3.4. *d-series comparison: fixing $Ro = Fr = 0.002$, varying δ*

The second series of flows we investigate was motivated by the question of how domain aspect-ratio could influence layer formation. The d-series includes d4, d8 and d16 ($\delta = 1/4, 1/8$ and $1/16$ respectively) in our database, all of which have $Fr \simeq 0.002$. In order to study the effect of varying δ while keeping as much of the rest of the parameter space fixed as possible, we chose to fix $Ro = Fr = 0.002$ such that the Burger number $Bu = Ro/Fr = \delta N/f = 1$ in all cases. Burger number unity flows are thought to be representative of mid-latitude ocean dynamics [45], hence the theoretical interest in such flows [1, 28]. In this section we focus on varying δ for fixed $Ro = Fr$. Choosing to fix $Bu = 1$ to study the effect of varying δ naturally affects N/f such that $N/f = 1/\delta \neq 1$ for these flows. All flows are in the quadratic potential enstrophy regime as shown in Fig. 1(b). Note that the potential enstrophy for the d-series saturates in time indicating that dissipation balances the downscale flux and that any upscale growth of potential enstrophy is absent.

Since early (equal) time comparisons of the three flows in this series are consistent with the late time descriptions below, we do not present the former. Fig. 9 shows the flow visualizations at the latest simulations times. In order that the structure thicknesses are clearly visible relative to the height of the domain, we show unit-aspect-ratio slices of the flows. For example, to visualize d16, which was computed on a $2048 \times 2048 \times 128$ grid, we show a 128×128 sub-section of a full 2048×128 y - z slice. In such a visualization the vertical scale thickness relative to the vertical domain height is made clear, but the extent of the horizontal scales are not. However, the latter are quantified later in the paper when we discuss the aspect-ratios of the internal scales; for now the reader should keep in mind the unavoidable bias in this choice of visual representation.

As in the B-series of runs, wave-mode layering is present in all three cases of the

d-series (Fig. 9 and the vertical thickness of the wave-modes appears to increase (relative to domain height) as N/f increases (δ decreases). At these latest times of the flows it appears to the eye that, relative to the vertical height of their respective domains, the vertical layer thickness does not change significantly from d4 to d16. If the latter simulations were run out to even longer times, it is possible that layers would develop. However, given the rather early time appearance of vortical layers in d16, it seems less likely that d8 and/or d4 would develop layers at much later times. It is difficult to make the assertion, from just these visualizations, that there is a strengthening of the vortical layers going from d8 to d16. In particular, the maximum amplitude of the velocity associated with the vortical modes in the visualizations appears to be decreasing as δ decreases, making it even harder to claim that the vortical mode layering is significant. Further quantification of the vertical and horizontal scales in the d-series occurs in Section 4. Note again that the visualizations themselves do not give an indication of the horizontal extent of the layers.

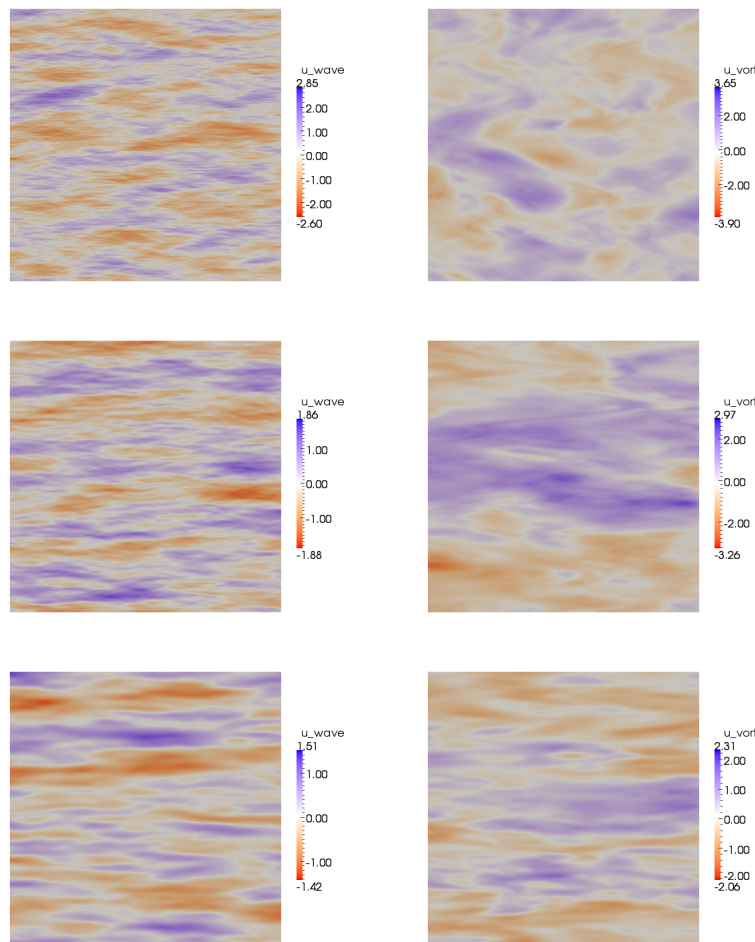


Figure 9. Visualization of a $(y-z)$ slice of the flow field at the latest time of the $Bu = 1$ small aspect-ratio simulations (d-series) showing iso-contours of the wave (left) and vortical (right) projection of \mathbf{u} . From top: $\delta = 1/4, N/f = 4$ (d4); $\delta = 1/8, N/f = 8$ (d8); and $\delta = 1/16, N/f = 16$ (d16). The wavenumbers $k \leq 5$ have been filtered out in all cases in order to focus on sub-forcing scales.

The total energy spectra for d4, d8 and d16 are shown in Fig. 10 with a k^{-2} line shown for comparison. There is a slight change in scaling at high wavenumbers for d4 but apart from that the overall energy scaling does not seem to change substantially going from $\delta = 1/4$ to $\delta = 1/16$ for fixed $Fr = 0.002$. The magnitudes

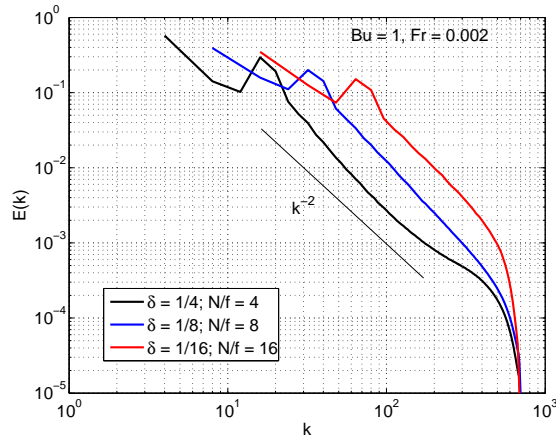
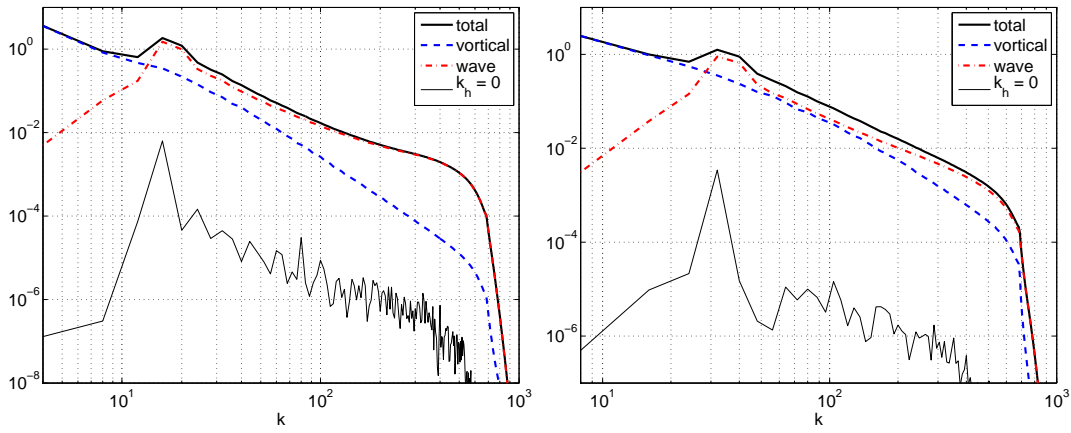


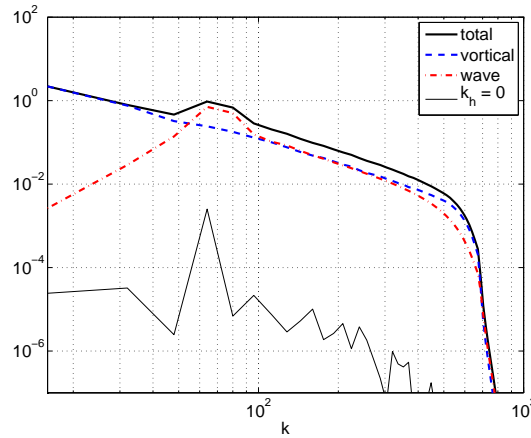
Figure 10. Comparison of the total energy spectra for all $Bu = 1$ flows showing that the decay rate in k has saturated.

of the spectra are different consistent with the shift in the peak of the forcing. The breakdown of the energy into the relevant components is shown in Fig. 11. In all cases, the VSHF never accumulate significantly at any scales, to be contrasted with VSHF growth in B4 and B8.



(a) d4: $\delta = 1/4; N/f = 4$.

(b) d8: $\delta = 1/8; N/f = 8$.



(c) d16: $\delta = 1/16; N/f = 16$.

Figure 11. The total, wave, vortical and $k_h = 0$ (wave) mode spectra for d-series flow ($Bu = 1$).

Numerical work by [9, 19] indicated that three-wave near-resonances are responsible for the generation of VSHF in strongly and purely stratified, unit aspect-ratio flows. Lack of VSHF in the d-series is consistent with the diminished role of three-wave near resonances for $Bu = 1$ irrespective of aspect-ratio [1]. In Fig. 11 the vortical energy has a k^{-3} decay rate for d4. The vortical mode energy becomes shallower and comparable to the wave energy over a wide range of wavenumbers as δ **decreases** in d8 and d16. Thus, while the relative contribution of the vortical energy grows as δ decreases, there is no evidence, for the δ values studied, that the vortical mode becomes dominant in the scales downscale from the forcing. At best, the vortical mode energy becomes comparable to the wave mode energy after long times for the smallest δ flow.

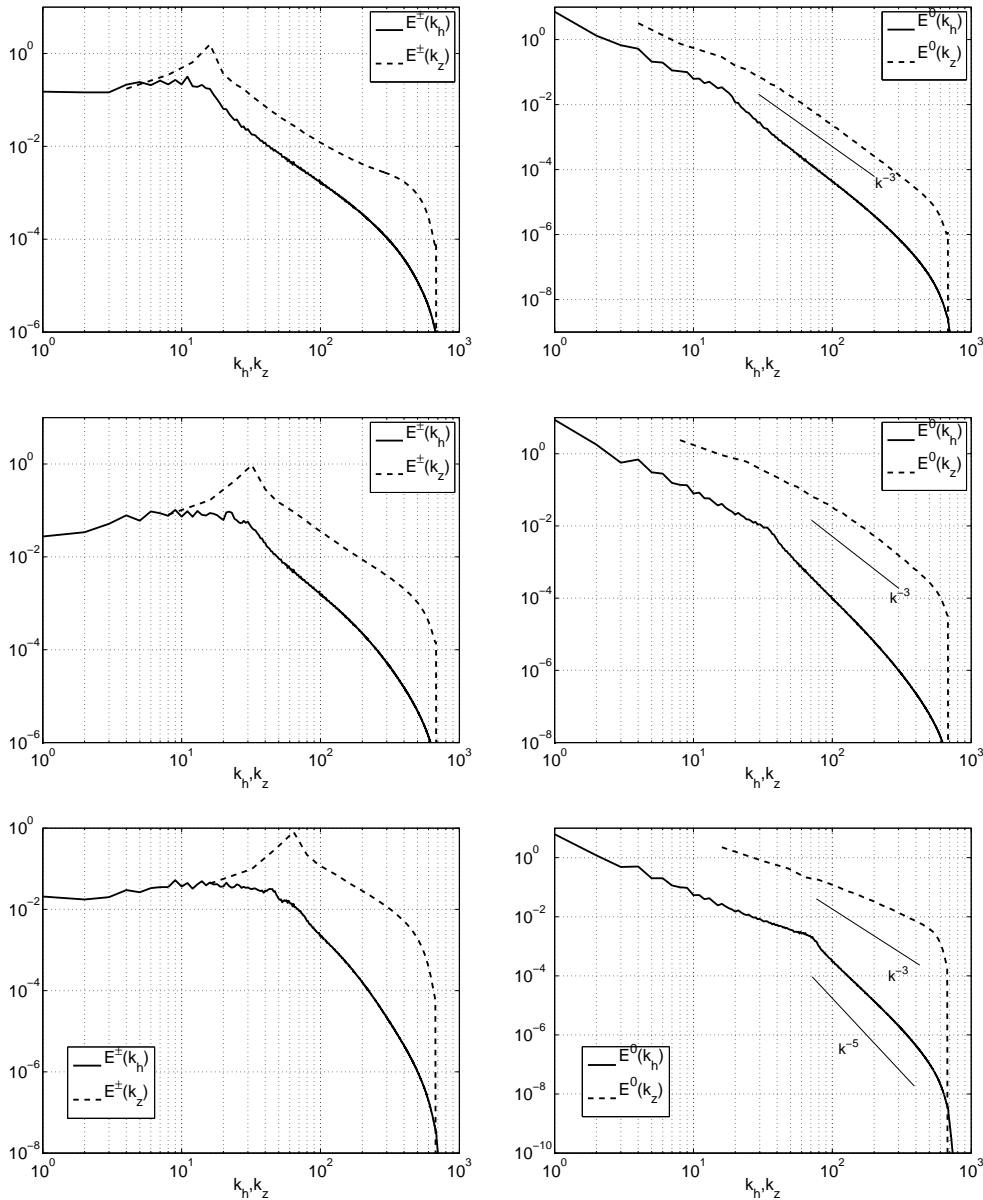


Figure 12. For the $Bu = 1$ flows, left column: wave energy as a function of k_h (solid) and k_z (dash). Right column: vortical energy as a function of k_h (solid) and k_z (dash). Top to bottom: $\delta = 1/4, 1/8, 1/16$ (d4, d8, d16).

As before, we consider the asymmetry of the spectra decomposed along k_h and k_z in Fig. 12. As δ decreases the the decay rate in k_h becomes much steeper than than

in k_z downscale of the forcing, for both wave and vortical modes. This asymmetry in the decay rates is consistent with layer formation. Not only is the vortical energy in k_h less than the vortical energy in k_z in all cases, but there is also a shallower scaling in k_z , consistent with finer scales in the vertical, in order to be consistent with layer formation. Even though d4, which does not exhibit strong vortical layers (Fig. 9) exhibits much less energy in the k_h modes than in the k_z (Fig. 12), but both curves scale similarly downscale from the forcing. Thus *asymmetry* in the decay rates of either wave or vortical energy with respect to k_h and k_z appears to be a signature of layer formation in that component.

The main conclusion from the d-series comparisons is that decreasing aspect-ratio for fixed small Fr and $Bu = 1$ leads to relatively weak vortical mode layering. The vortical mode energy becomes comparable to the wave mode energy at sub-forcing scales, but does not dominate the energy even at our smallest $\delta = 1/16$ (to be contrasted with B16, also at $N/f = 16$, in which vortical energy dominates). We do not have data at even smaller δ to assert whether or not the vortical mode energy becomes dominant as for the unit aspect-ratio case with small Fr and increasing Ro .

3.5. Comparison between B-series and d-series: for fixed $Fr \simeq 0.002$, fix N/f and vary δ

A final comparison may be made between the $\delta = 1$ flow and the $\delta = f/N$ flow, for fixed $Fr_o = 0.002$ for each value of $N/f = 4, 8$ and 16 . That is, we can compare pairwise: B4 with d4, B8 with d8, and B16 with d16. Note again that Ro is not fixed in these pair-wise comparisons. We have already shown and discussed the VSHF in terms of their presence in Bn flows and absence in the dn flows, that discussion will not be repeated here.

The first difference for fixed N/f lies in the potential enstrophy evolution itself, as has been noted before. For fixed $1 < N/f \leq 32$ the corresponding B-series flow has growing potential enstrophy for B4, B8, and B16, while the d-series flows achieved statistically steady potential enstrophy in all cases. Thus, for fixed $4 \leq N/f \leq 32$ the potential enstrophy is allowed to grow upscale or accumulate at certain scales in the unit aspect-ratio domain, but transfers entirely downscale and is dissipated for small aspect-ratio.

In a side-by-side comparison of the physical structure of flows for fixed $N/f = 16$, we reproduce here some visualizations from earlier in the paper in Fig. 13. (The comparisons for $N/f = 4, 8$ are qualitatively the same and therefore $N/f = 16$ is taken to be representative.) There is clear wave-mode layering for fixed $N/f = 16$ for both unit and small aspect-ratio. However, fine-scale structure is less prevalent for d16 as compared to B16, the latter displaying horizontally more extended and smoother layers. There appear to be much weaker layers (if any) in the vortical component for d16 compared to B16. By ‘weaker’ we mean that the vortical layers in d16 are less pronounced in the visualization than the layers in B16; and the magnitude of the vortical component visualized is relatively smaller in magnitude in d16 compared to B16. If vortical mode layering is taken to be a signature of stratification dominated flows [5], then one might describe the small aspect-ratio cases as being less strongly stratified than the unit aspect-ratio cases for fixed N/f .

Finally, we measure the degree to which the vortical component contributes to the total energy in the sub-forcing scales. Consider the ratio of total vortical energy $E_{>}^0$ in wavenumbers $k_f + 5 < k < k_{max}$ to the total energy $E_{>}$ in the same wavenumber range, in both small and unit-aspect-ratio runs, comparing flows with equal N/f . In Fig. 14 we see that for fixed $Bu = 1$ as N/f increases from 4 to 16 (with aspect-

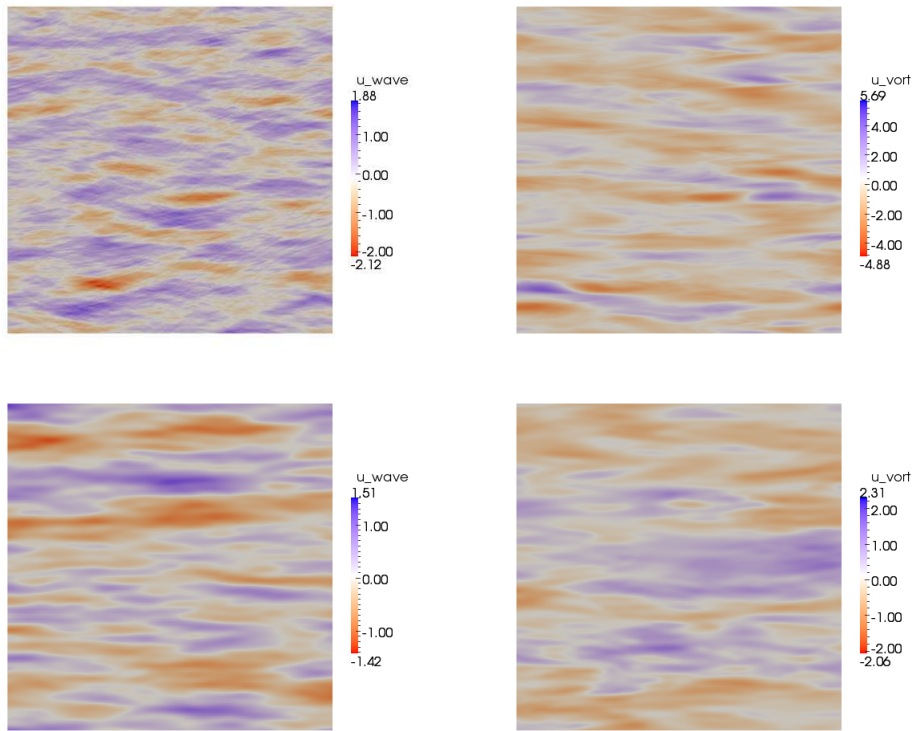


Figure 13. Comparison of visualization of u^\pm (left) and u^0 (right) for two $N/f = 16$ flows B16 (top) and d16 (bottom).

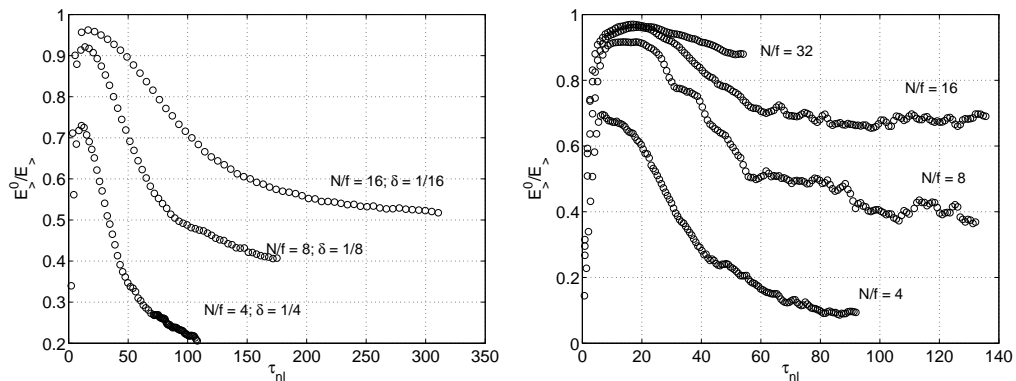


Figure 14. Ratio of total vortical energy to total energy in the subforcing $k > k_f + 5$ scales. Left: Small aspect-ratio runs with fixed $Bu = 1$ and increasing N/f . Right: Unit aspect-ratio runs with increasing N/f .

ratio decreasing accordingly from 1/4 to 1/16), the ratio $E^0_{>}/E_{>}$ grows from 20% to 50%. Thus the vortical mode energy becomes, at best, comparable to the wave energy at the largest value of $N/f = 16$. By contrast, for fixed $\delta = 1$ as N/f increases from 4 to 16, the ratio $E^0_{>}/E_{>}$ grows from 10% to 70% (and up to nearly 90% for $N/f = 32$). This is a quantitative way to show that growth of the vortical energy relative to the total energy appears suppressed in the small aspect-ratio flow relative for the unit aspect-ratio flow as N/f increases, a point which has been made earlier.

4. Quantitative trends in the internal lengthscales

A standard way to quantify emergent lengthscales in flows has been the use of correlation length (in physical space), or equivalently the centroid of the power spectrum. There are two caveats in using such a measure in the present context. First, since the flow is forced, the forcing scale inevitably weights such a measure. Second, such measures are often not commensurate with our recognition, from the flow visualizations, of the apparent multiscale nature of the layered structure.

Given these caveats we nevertheless attempt to extract trends in the parameter space for vertical and horizontal correlation length scales, in both vortical and wave components. The scales are defined as follows:

$$\begin{aligned}
 H_{0[\pm]} &= 2\pi \left(\frac{\sum_{k_z=0}^{k_z^{max}} k_z E^{0[\pm]}(k_z) \Delta k_z}{E^{0[\pm]}} \right)^{-1} \\
 L_{0[\pm]} &= 2\pi \left(\frac{\sum_{k_h=0}^{k_h^{max}} k_h E^{0[\pm]}(k_h) \Delta k_h}{E^{0[\pm]}} \right)^{-1} \\
 \delta_{0[\pm]} &= \frac{H_{0[\pm]}}{L_{0[\pm]}}
 \end{aligned} \tag{13}$$

where $H_{0[\pm]}$ and $L_{0[\pm]}$ are the correlation lengths in the vertical and horizontal respectively, of the vortical[wave] component. Similar quantities were defined for the vortical modes in [13]. In the discussion to follow, we will often distinguish between what we term *absolute* quantities H_0 and δ_0 , and *relative* quantities H_0/H_d and δ_0/δ . The relative quantities are useful when considering the emergent scales relative to the domain scales for small aspect-ratio domains. Absolute and relative scales are of course identical for the unit aspect-ratio cases. To avoid the proliferation of related plots we present the measured vertical scales and the internal aspect-ratios with the understanding that the latter is derived from the measured horizontal scales as in equations 13.

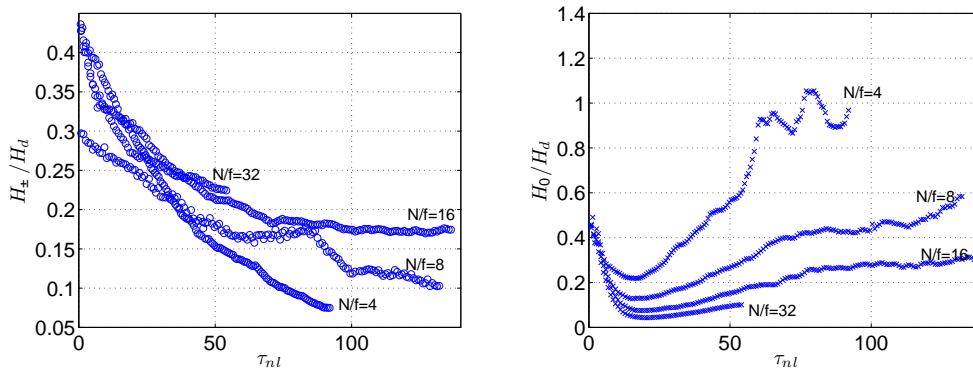


Figure 15. Wave (left) and vortical (right) vertical correlation lengths for the B-series, unit-aspect ratio flows.

The vertical correlation lengths of the wave and vortical components of the flow, are presented for the B-series in Fig. 15. For the wave component, after about $\tau = 50$, the vertical length scale increases from about 8% for $N/f = 4$ to 22% for $N/f = 32$. For the vortical component, the trend is the opposite; for $N/f = 4$ the vertical length scale is comparable to the domain height indicating weak, if any, layered structure, and as N/f increases to 32 the relative vertical correlation length decreases to as low as 10%. Both results in Fig 15 are consistent with our more

qualitative results from visualizations and spectra for the B-series in the sections above. In addition, the decrease in the vortical scale thickness is also consistent with [13] wherein the overall vertical scale was shown to decrease as N/f increased in a comparable series of flows.

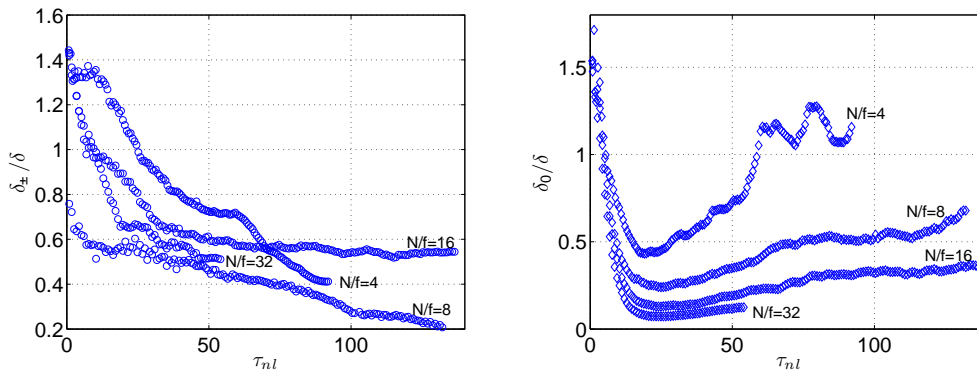


Figure 16. Wave (left) and vortical (right) correlation aspect-ratios for the B-series, unit-aspect ratio flows.

Another measure of the distortion of the scales occurs relative to the domain aspect-ratio. In Fig. 16 we show the internal aspect-ratio of the B-series flows. There is no consistent trend in the wave-component going from $N/f = 4$ to $N/f = 32$. The intermediate $N/f = 8$ and 16 are consistent with the growth and diminishment of the VSHF observed in these flows as N/f is varied. The VSHF, when they appear, can extend horizontally over the entire domain thus biasing the horizontal correlations and consequently the aspect-ratios δ_{\pm} . The aspect-ratio of the vortical component of the B-series on the other hand shows a much clearer trend, decreasing as N/f increases. That is, the structures go from having an aspect-ratio nearly 1 at $N/f = 4$ (that, is no layering in the vortical mode) to having aspect-ratio 15% for $N/f = 32$.

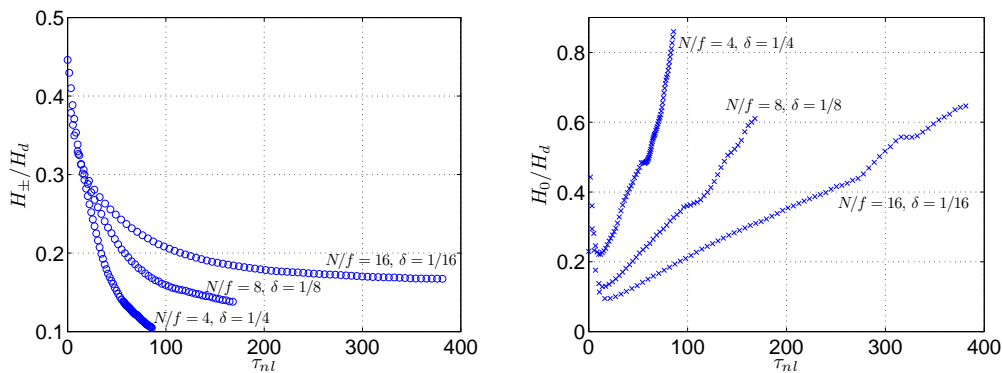


Figure 17. Wave (left) and vortical (right) vertical correlation lengths relative to the vertical domain size for the d-series, with fixed $Bu = 1$.

In a similar analysis of the d-series flows with fixed $Bu = 1$, we see in Fig. 17, the *relative* vertical correlation length of the wave-mode becomes larger as N/f is increased (domain aspect-ratio is decreased). Qualitatively, these observations are comparable to those for the B-series between flows of the same N/f . Indeed for both series of flows, the wave-component value of H_{\pm}/H_d increases from $\approx 10\%$ to $\approx 17.5\%$ as N/f increases from 4 to 16, indicating that the relative thickness of structures in the wave-component of the flow is governed largely by N/f , irrespective of aspect-ratio.

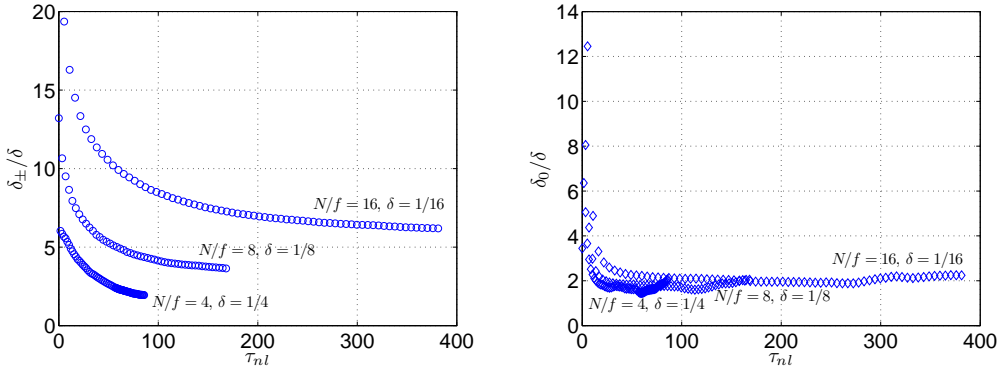


Figure 18. Wave (left) and vortical (right) correlation aspect-ratios for the d-series, $Bu = 1$ flows.

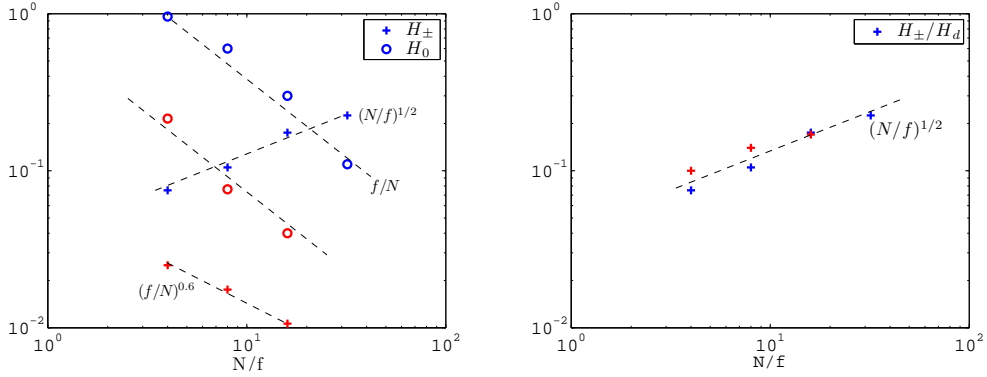


Figure 19. Left: Absolute vertical scale thickness of wave (+) and vortical (o) modes as a function of N/f . Right: Relative vertical scale thickness for wave (+) modes as a function of N/f . In both panels, dashed lines indicate scalings in N/f , blue symbols indicate B-series, red symbols indicate d-series.

In the right panel of Fig. 17, the relative vertical scale of the vortical component decreases as N/f is increased (δ decreased). This is qualitatively similar to the B-series for the same N/f , although the vortical mode scales in the d-series are still strongly growing in time. Let us choose equal nonlinear times of about $\tau = 100$: H_0/H_d drops from $\mathcal{O}(1)$ to about 30% as N/f increases from 4 to 16 in the B-series, and from about 85% to about 25% for the same drop in N/f in the d-series. If we choose the latest times of the respective flows instead, then the change remains the same for the B-series (since those correlation lengths have more or less saturated in time), but goes from about 90% to about 65% in the d-series.

The internal aspect-ratios of the d-series are shown in Fig. 18. The wave component shows an increase in the relative aspect-ratio δ_{\pm}/δ from 2 to 6 as N/f increases from 4 to 16. A value of $\delta_{\pm[0]}/\delta > 1$ indicates that the structures in a flow are not as ‘flat’ as the domain. By this measure, the aspect-ratio of the wave-modes relative to the domain-aspect ratio in the d-series does increase relative to the domain aspect-ratio, but the structures themselves are less flat than the domain itself. Notably the same measure in the vortical modes (Fig. 18)(b) shows that δ_0/δ seems to converge to 2 irrespective of N/f (or δ) for the d-series $Bu = 1$ flows. Therefore we may conclude that the relative aspect-ratio of the vortical mode might be fixed by the Bu number alone for both the B and d-series flows. Although to confirm this, we would need more parameter studies with small aspect-ratio $Bu > 1$ flows, which we do not have.

The dependence of the internal (emergent) scales on the variation of N/f is given in Fig. 19. We use the latest time data, and have four data-points for the B-series and three in the d-series and therefore need to exert some caution in discerning

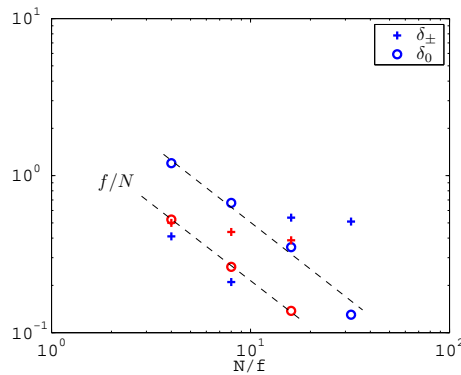


Figure 20. Aspect-ratio of wave (+) and vortical (o) modes as a function of N/f . Dashed lines indicate scalings in N/f , blue symbols indicate B-series, red symbols indicate d-series.

trends and making extrapolations. In the left panel, $H_0 \sim f/N$ for both the B-series and the d-series. This is consistent with the visualizations of the B series (Fig. 6) which clearly show decreasing thickness of the vortical layers as N/f increases. It is also consistent with the apparent lack of change of the *relative* thickness of the vortical layers in the d-series (Fig. 9) since more generally, $H_0 \sim f/N \Rightarrow H_0/H_d \sim Bu^{-1}$.

The monotonic decrease of the vortical mode thickness with increasing N/f is consistent with the observations of [13, 22] in unit aspect-ratio strongly stratified flows with $Ro \ll 1$. In flows which were forced only in the vortical component, [13] observed vortical mode layer thickness scales with fL/N in rotating stratified Boussinesq turbulence for $Ro < 1$. Although we also forced the wave-modes, our results are in agreement with this aspect of [13]. For stratified flow dominated by vortical motion with $Ro > 1$, [13] also observed the vortical mode layer thickness scaling with U_h/N , where U_h is a characteristic horizontal velocity; we do not address this latter regime. The experimental work of [22] on rotating and stratified flow with turbulence, found that the aspect-ratio of internal eddies decreases monotonically with f/N as the turbulence decayed. They measured the internal aspect-ratio using vertical and horizontal Taylor microscales and did not separate the vortical modes of the flow. Furthermore, the decrease in aspect-ratio observed in [22] was not a linear function of f/N , indicating corrections from quasi-geostrophic theory. Departures from f/N scaling of the characteristic scales have been of interest recently, for example in studies of laboratory vortices [46, 47]. Given our results for the wave-component scales below, we propose that corrections to the quasi-geostrophic scaling may arise due to wave-mode contributions.

In the same Fig. 19, H_{\pm} grows as $(N/f)^{0.5}$ for the B-series and decays roughly as $\sim (N/f)^{-0.6}$ for d-series flows. However the *relative* wave-mode vertical scales in the right panel of Fig. 19, indicate very rough scaling of $(N/f)^{0.5}$, independent of δ . Even given the sparsity of data, the main point is that, in contrast to the vortical modes, the *relative* vertical scale of the wave mode *increases* monotonically with N/f with scaling exponent of around 0.5. For ease of subsequent discussion we will use the 0.5 scaling exponent as an approximate power, asking the reader to keep in mind the caveats.

In Fig. 20 we see that δ_0 decreases as f/N for both the B-series and the d-series. Equivalently, δ_0/δ decreases as Bu^{-1} , identical to the scaling of H_0/H_d . This is because the horizontal lengthscale L_0/L_d (not shown) is independent of N/f and δ . In the same figure δ_{\pm} for the B-series exhibits some scatter as a function of N/f , likely due to the anomaly introduced by the VSHF; however the overall trend is consistent with a constant function of N/f . For the d-series also there is weak to

no dependence of δ_{\pm} on N/f , or $\delta_{\pm}/\delta \sim \delta^{-1}$. This in combination with the fact that H_{\pm} grows as $\sim (N/f)^{1/2}$, is because the relative horizontal lengthscale L_{\pm}/L_d (not shown) grows roughly as $(N/f)^{1/2}$.

To our knowledge, such a dissection of the correlation lengths of the vortical and wave modes has not been reported previously. The Bu^{-1} scaling with increasing N/f observed for both the relative vertical scales and the relative aspect-ratios of the vortical modes seems to be quite robust under change in aspect-ratio. Even the data which do not have dominant vortical modes (B4 and B8) lie on this trend. However the slow *growth* of the (relative) vertical correlation length of the wave-modes as N/f increases can become dominant for large N/f , even when the wave-mode energy itself is subdominant. In Fig. 19 we see that at $N/f = 32$, H_{\pm} is larger than H_0 for the B-series, even though vortical energy dominates that flow (see for example Fig. 4b). Thus a gross calculation of the characteristic layer thickness, presumably a non-trivial combination of H_0 and H_{\pm} , could show departures from Bu^{-1} behavior.

run	δ_0/δ	δ_{\pm}/δ	Bu	Bu_0	Bu_{\pm}
B4	1.2	0.41	4	4.8	1.68
B8	0.67	0.21	8	5.76	1.76
B16	0.35	0.54	16	5.92	8.8
B32	0.13	0.51	32	4.16	16.64
d4	2.1	2	1	2.1	2
d8	2.1	3.5	1	2.1	3.5
d16	2.2	6.2	1	2.2	6.2

Table 2. Relative aspect-ratios and corresponding Burger numbers for the vortical and wave modes at latest times. For reference, the global Burger Bu is repeated here for each flow.

It is worthwhile to note that calculation of a Burger number based on the intrinsic final scales of these flows is now possible. Define a vortical Burger number $Bu_0 = \delta_0 N/f = Bu \delta_0/\delta$ and a wave Burger number $Bu_{\pm} = \delta_{\pm} N/f = Bu \delta_{\pm}/\delta$. Based on the latest value in time of the relative aspect-ratios, these internal Burger number values are tabulated across various flows in Table 2. While these values of $Bu_{0[\pm]}$ are different from the global Bu we defined at the outset of this study, the two are comparable in many cases. Bu_0 varies between about 4 and about 6 for the B-series as the Bu varies from 4 to 32. This indicates that the “effective” stratification of the vortical mode is less than what the global parameters indicate for the B-series. Bu_{\pm} on the other hand varies from $\mathcal{O}(1)$ to about 16 as Bu varies from 4 to 32 in the B-series indicating much stronger stratification of the wave mode as compared to the vortical mode. The vortical mode dominates the energy but the stratification, as measured by scale distortion and internal Burger number is stronger in the wave-mode.

For the d-series Bu_0 is remarkably constant, (equal to 2), consistent with, though indicative of somewhat stronger stratification than, the globally constant $Bu = 1$. $Bu_0 = 2$ also indicates less stratification than flow with comparable N/f in the B-series. In the d-series Bu_{\pm} varies from 2 to 6.2 which indicates stronger stratification than the global $Bu \sim \mathcal{O}(1)$ would indicate, but still weaker than the B-series flow with comparable N/f . Again, consistent with more qualitative statements above, these analyses show that the stratification effects, measured by scale distortion as described, is stronger in the wave mode than in the vortical mode for all flows in our study; and for a given N/f the small aspect-ratio cases display weaker stratification than the unit aspect-ratio cases.

5. Summary

Our intention in this study was to attempt to disentangle the effects of N/f , Fr , Ro , δ and Bu , the classical parameters of rotating and stratified flows. Our point of comparison was structure formation and its quantitative representation in energy spectra. A standard systematic parameter study, that is, varying a single parameter at a time keeping all others fixed, was impossible because of how they are linked. We have nevertheless performed several scans of the parameter space varying as little in each scan as possible. The parameter that remained fixed across all flows was the low $Fr = Fr_o \simeq 0.002$ which ensured quadratic potential enstrophy, and reduced non-dimensional stratification to a fixed but strong background effect. This strong stratification also makes the Reynolds number irrelevant in that the wave-overturning and turbulent overturning is completely suppressed, further narrowing the possible parameter space.

On this fixed 'background' we first set $\delta = 1$ and varied Ro (f) from $Ro = Fr$ to larger values. The conclusions were that growth in Ro is responsible for delaying and/or suppressing the appearance of VSHF in the small scales. The wave modes (apart from the VSHF) showed layering at all values of Ro with diminishing fine-scale structure as Ro increased. The vortical modes appear to transition from a non-layered (or weakly layered) structure at $Ro \simeq 4Fr$ and then to strong layers with increasing fine-scale structure as Ro is increased further. The spectra correspondingly showed a transition in which the vortical energy dominated the small-scales as Ro increased. The utility of using the wave-vortical decomposition and associated energy spectra to dissect the structures in this manner was evident particularly because the total spectra were not very different in all cases for this part of the study.

The difficulties introduced with δ as a variable are apparent in the definition of $Bu = Ro/Fr = N\delta/f$. The variation of δ would result in either Bu varying for fixed N/f , or vice versa. We chose the latter and fixed $Bu = 1$ in deference to known theory and empirical parameters for parts of the ocean. This choice along with our $\delta = 1$ data, allows two additional studies – decreasing δ for fixed $Bu = 1$ and decreasing δ for fixed N/f . The effect in both comparisons, broadly speaking, is to suppress fine-scale structure in the vertical relative to the domain height for the vortical mode.

The measurement of correlation lengths and internal aspect-ratios refines what has been learned from visualizations and energy spectra. An interesting result, robust across all runs, is the observation that the vortical-mode internal aspect-ratio decays nearly linearly with f/N . In our simulations, the wave-mode internal aspect-ratio is roughly constant with f/N . Of course the net characteristic scales of a flow depend on the vortical-mode and wave-mode contributions together. It is possible that the departures from f/N scaling of internal aspect ratios observed in other settings (e.g. [22]) could be attributed to contributions from the wave modes. To refine this hypothesis further, more simulations and analyses matching the parameters and measurements of [22] would be required.

It must be noted that in many of the cases we studied, the flow is continuing to evolve (for example the d-series vortical modes), and our comparisons are for different non-dimensional end times. Furthermore, as previously noted, there is significant under-resolution of the buoyancy scale in d-series flows, unavoidable by our choice to fix Fr and our finite computational resources. Whether or not the scalings of the vertical scales and internal aspect ratios persist under improved resolution is a topic for future research.

Acknowledgements

We used resources of the Argonne Leadership Computing Facility at Argonne National Laboratory, supported by the Office of Science of the US DOE under Contract No. DE-AC02-06CH11357. SK and LMS received partial funding from NSF program Collaborations in the Mathematical Geosciences: NSF CMG-1025188 (SK was funded via the New Mexico Consortium). This research was performed under the auspices of the US DOE at LANL under Contract No. DE-AC52-06NA25396.

References

- [1] A. Babin, A. Mahalov, B. Nicolaenko, and Y. Zhou, *On the asymptotic regimes and the strongly stratified limit of rotating Boussinesq equations*, Theoret. Comput. Fluid Dyn. 9 (1997), p. 223.
- [2] B. Cushman-Roisin *Introduction to Geophysical Fluid Dynamics*, Prentice-Hall, Eaglewood Cliffs, NJ, USA, 1994.
- [3] J. Riley, R. Metcalfe, and M. Weissman, *Direct numerical simulations of homogeneous turbulence in density-stratified fluids*, Nonlinear Properties of Internal Waves, AIP (1981), pp. 79–112.
- [4] E.J. Hopfinger, F.K. Browand, and Y. Gagne, *Turbulence and waves in a rotating tank*, J. Fluid Mech. 125 (1982), pp. 505–534.
- [5] D. Lilly, *Stratified Turbulence and the Mesoscale Variability of the Atmosphere*, J. Atmos. Sci. 40 (1983), pp. 749–761.
- [6] O. Metais, and J. Herring, *Numerical studies of freely decaying homogeneous stratified turbulence*, J. Fluid Mech. 202 (1989), pp. 117–148.
- [7] P. Bartello, O. Metais, and M. Lesieur, *Coherent structures in rotating three-dimensional turbulence*, J. Fluid Mech. 273 (1994), pp. 1–29.
- [8] L. Smith, and F. Waleffe, *Transfer of energy to two-dimensional large scales in forced, rotating three-dimensional turbulence*, Phys. Fluids 11 (1999), pp. 1608–1622.
- [9] L. Smith, and F. Waleffe, *Generation of slow, large scales in forced rotating, stratified turbulence*, J. Fluid Mech. 451 (2002), pp. 145–168.
- [10] J.J. Riley, and S.M. Bruyn Kopsde, *Dynamics of turbulence strongly influenced by buoyancy*, Phys. Fluids 15 (2003), p. 2047.
- [11] L. Smith, and Y. Lee, *On near resonances and symmetry breaking in forced rotating flows at moderate Rossby number*, J. Fluid Mech. 535 (2005), pp. 111–142.
- [12] F.M. C. Morize, and M. Rabaud, *Decaying grid-generated turbulence in a rotating tank*, Phys. Fluids 17 (2005), p. 095105.
- [13] M. Waite, and P. Bartello, *The transition from geostrophic to stratified turbulence*, J. Fluid Mech. 568 (2006), pp. 89–108.
- [14] G. Brethouwer, P. Billant, E. Lindborg, and J. Chomaz, *Scaling analysis and simulation of strongly stratified turbulent flows*, J. Fluid Mech. 28 (2007), pp. 343–368.
- [15] L. Bourouiba, and P. Bartello, *The intermediate Rossby number range and two-dimensional-three-dimensional transfers in rotating decaying homogeneous turbulence*, J. Fluid Mech. 587 (2007), pp. 139–161.
- [16] B. Sreenivasan, and P. Davidson, *On the formation of cyclones and anticyclones in a rotating fluid*, Phys. Fluids 20 (2008), p. 085104.
- [17] M. Waite, *Stratified turbulence at the buoyancy scale*, Phys. Fluids 23 (2011), p. 066602.
- [18] P. Augier, J.M. Chomaz, and P. Billant, *Spectral analysis of the transition to turbulence from a dipole in stratified fluid*, Journal of Fluid Mechanics 713 (2012), pp. 86–108.
- [19] M. Rempel, J. Sukhatme, and L. Smith, *Nonlinear gravity wave interactions in stratified turbulence*, Theor. Comp. Fluid Dyn. (2013).
- [20] M. Waite, *Potential enstrophy in stratified turbulence*, J. Fluid Mech. 722 (2013), p. 066602.
- [21] O. Praud, A.M. Fincham, and J. Sommeria, *Decaying grid turbulence in a strongly stratified fluid*, Journal of Fluid Mechanics 522 (2005), pp. 1–33.
- [22] O. Praud, J. Sommeria, and A.M. Fincham, *Decaying grid turbulence in a rotating stratified fluid*, J. Fluid. Mech 547 (2006), pp. 389–412.
- [23] H. Ertel, *Ein Neuer hydrodynamischer Wirbelsatz*, Met. Z. 59 (1942), pp. 271–281.
- [24] J. Charney, *Geostrophic turbulence*, J. Atmos. Sci. 28 (1971), pp. 1087–1095.
- [25] P. Embid, and A. Majda, *Low Froude number limiting dynamics for stably stratified flow with small or finite Rossby numbers*, Geophys. Astrophys. Fluid Dyn. 87 (1998), pp. 1–50.
- [26] J.P. Laval, J. McWilliams, and B. Dubrulle, *Forced Stratified Turbulence: Successive Transitions with Reynolds Number*, Phys. Rev. E 68 (2003), p. 036308.
- [27] M. Waite, and P. Bartello, *Stratified Turbulence Generated by Internal Gravity Waves*, J. Fluid Mech. 546 (2006), pp. 313–339.
- [28] A. Babin, A. Mahalov, and B. Nicolaenko, *Fast singular oscillating limits and global regularity for the 3D primitive equations of geophysics*, Math. Modelling and Num. Analysis 34 (2000), pp. 201–222.
- [29] M. Rempel, and L.M. Smith, *New intermediate models for rotating shallow water and an investigation of the preference for anticyclones*, J. Fluid Mech. 635 (2009), pp. 321–359.
- [30] S. Kurien, L. Smith, and B. Wingate, *On the two-point correlation of potential vorticity in rotating and stratified turbulence.*, J. Fluid Mech. 555 (2006), pp. 131 – 40.
- [31] S. Kurien, B. Wingate, and M. Taylor, *Anisotropic constraints on energy distribution in rotating and stratified flows*, Europhys. Lett. 84 (2008), p. 24003.

- [32] H. Aluie, and S. Kurien, *Joint downscale fluxes of energy and potential enstrophy in rotating and stratified Boussinesq flows*, Europhys. Lett. 96 (2011), p. 44006.
- [33] S. Kurien, and L. Smith, *Asymptotics of unit Burger number rotating and stratified flows for small aspect-ratio*, Physica D: Nonlinear Phenomena 241 (2012), pp. 149–163.
- [34] G. Nastrom, and K. Gage, *A climatology of aircraft wavenumber spectra observed by commercial aircraft*, J. Atmos. Sci. 42 (1985), pp. 950–960.
- [35] E. Lindborg, *The energy cascade in a strongly stratified fluid*, Journal of Fluid Mechanics 550 (2006), pp. 207 – 42.
- [36] A. Gill *Atmosphere-Ocean Dynamics*, International Geophysics Series Academic Press, 1981.
- [37] A. Majda *Introduction to PDEs and waves for the atmosphere and ocean*, Courant Lecture Notes in Mathematics Vol. 9, New York University Courant Institute of Mathematical Sciences, New York, 2003.
- [38] G. Vallis *Atmospheric and Oceanic Fluid Dynamics*, Cambridge University Press, Cambridge, 2006.
- [39] E. Spiegel, and G. Veronis, *On the Boussinesq approximation for a compressible fluid*, Astrophysical Journal 131 (1960), pp. 442–447.
- [40] P. Bartello, *Geostrophic adjustment and inverse cascades in rotating stratified turbulence*, J. Atmos. Sci. 52 (1995), pp. 4410–4428.
- [41] J. Sukhatme, and L. Smith, *Vortical and wave modes in 3D rotating stratified flows: Random large scale forcing*, Geophys. Astrophys. Fluid Dyn. 102 (2008), p. 437.
- [42] M. Rempel, J. Sukhatme, and L.M. Smith, *Nonlinear inertia-gravity wave-mode interactions in three dimensional rotating stratified flows*, Commun. Math. Sci. 8 (2010), pp. 357–376.
- [43] E. Lindborg, *Third-order structure function relations for quasi-geostrophic turbulence*, Journal of Fluid Mechanics 572 (2007), pp. 255 – 60.
- [44] M. Waite, and P. Bartello, *Stratified turbulence dominated by vortical motion*, J. Fluid Mech. 517 (2004), pp. 281–308.
- [45] J. McWilliams, *A note on a uniformly valid model spanning the regimes of geostrophic and isotropic, stratified turbulence: balanced turbulence*, J. Atmos. Sci. 42 (1985), pp. 1773–1774.
- [46] O. Aubert, M. Le Bars, P. Le Gal, and P.S. Marcus, *The universal aspect ratio of vortices in rotating stratified flows: experiments and observations*, J. Fluid. Mech 706 (2012), pp. 34–45.
- [47] P. Hassanzadeh, P.S. Marcus, and P. Le Gal, *The universal aspect ratio of vortices in rotating stratified flows: theory and simulation*, J. Fluid. Mech 706 (2012), pp. 46–57.